NTNU
Norwegian University of Science and Technology

endurcrete

Carbonation resistance of concrete and mortar containing novel low clinker cement

Specialization project in concrete technology

By Marie Helene Bjørndal

Preface

This report presents a study on carbonation resistance of new cement compositions introduced in the EU Horizon 2020 project, EnDurCrete. The project's main goal is to develop a new cost-effective and sustainable concrete, based on low clinker cement containing high value industrial by-products. The project has received funding from the European Union's Horizon 2020 research and innovation programme under grant agreement No. 760639 "EnDurCrete".

This paper will function as preparation for the upcoming master thesis, which will include further studies of the durability of the EnDurCrete binders, focusing on chloride ingress. The master's thesis conclude the master's degree program of Civil and Environmental Engineering at NTNU with specialization in concrete technology.

The work is based on the curriculum of TKT4235 Concrete technology advanced course and self study, and is performed in close collaboration with my supervisors, professor Klaartje De Weerdt and post doc Alisa Machner. I would like to thank my supervisors for inspiring and motivating me by offering helpful guidance and always showing great interest in my work.

Disclaimer: the report reflects the author's views. The European Commission is not responsible for use of the information in the report.

Trondheim, September 2019
Marie Helene Bjørndal

Student at Department of Structural Engineering, NTNU

Acknowledgements

I would like to thank Jan Lindgård, senior research scientist at SINTEF Community, for his helpful input and guidance in the preparations for the relative humidity measurements performed in the project. Thank you to Egil Rognvik, senior engineer at SINTEF Community, for calibrating the equipment needed for the relative humidity measurements.

I would like to thank Andrei Shpak, PhD candidate at Department of Structural Engineering at NTNU, for helping us prepare the samples for exposure in the carbonation chamber.

I would like to thank project partner, Acciona, for preparing the samples used in the project.

Abstract

Corrosion of reinforcement steel is a major deterioration mechanism for reinforced concrete structures. Corrosion can be caused by the carbonation of concrete. In this report we test the carbonation resistance of a novel low clinker cement with ground granulated blast-furnace slag (GGBFS) and limestone developed in the EnDurCrete project (CEMII/C-M(S-LL)), by comparing its performance to an already commercially available blended cement (CEMII/A-S). We determine and compare the ingress of the carbonation front under accelerated laboratory conditions (1% CO_2, 60% RH) on both mortar and concrete, for both cements, after 14, 28 and 90 days. We estimate the carbonation depth using two different techniques: thymolphtalein pH indicator and portlandite profiles determined by thermogravimetric analysis (TGA). In addition, we determine the relative humidity in the samples prior to exposure. The average RH for the mortar and concrete samples prior to exposure was similar. This suggests that mortar samples can be used to describe the moisture state in concrete. The RH ranged between 88 and 92%, which agrees with the level one would obtain by self-desiccation in sealed samples. The portlandite content in the non-carbonated EnDurCrete mortar is lower compared to the reference mortar, as can be expected due to the higher replacement levels with GGBFS. A lower carbonation resistance could be expected because of this, however this was not the case for the concrete samples. The carbonation depth determined by the pH indicator and the portlandite profiles agree well, taking into account the different ways of sampling for the two methods. The carbonation ingress results for mortar and concrete agree well, except for the reference mortar samples which showed a lower carbonation ingress. The reason for this is unknown. Based on the carbonation ingress results obtained on concrete, the EnDurCrete concrete exhibits a similar carbonation resistance as the reference concrete with the commercially available cement. This indicates the possibility to introduce the EnDurCrete cement as a valuable alternative to commercially available cements, providing similar properties and substantial reduction in greenhouse gases during production.

Table of contents

1. Background and theoretical basis

In this report we will study the carbonation resistance of a novel low clinker binder that aims to limit the CO_2 emissions from the cement production, hence a short background on environmental challenges in cement production, cement hydration and carbonation is provided.

1.1. Environmental challenges in cement production

The cement production industry is responsible for up to 8 % of the global CO2 emissions [1], releasing about 1 tonne CO2 per tonne clinker produced according to Norcem [2]. The emissions come from the decomposition of limestone during calcination (Equation 1) [3], as well as fuel combustion for heating up the raw meal in the kiln. This means that efficient energy use alone is not sufficient to make a significant impact on the emissions [4]. In order to reduce emissions it is necessary to find new cement compositions that require less limestone to be calcined, while maintaining good properties with regards to mechanical properties and durability.

$$CaCO_3 \rightarrow CaO + CO_2 \quad (1)$$

1.2. Cement hydration

The hydration process is the collection of chemical reactions between cement minerals and water, resulting in the setting and hardening of concrete. The binder properties of a cement is determined by the content of different clinker minerals and their fineness, and the content of supplementary cementitous materials (SCMs) [5]. The mineralogical names, cement chemistry abbreviations, formulas and chemical names of the major clinker phases are presentented in Table 1. SCMs are silica containing materials that, if finely divided and in the presence of hydration products and moisture, form products with binder properties.

Table 1 The mineralogical name, cement chemistry notation, formula and chemical name for the four major clinker phases.

Mineralogical name	**Cement chemistry notation**	**Formula**	**Chemical name**
Alite	C_3S	$3CaO{\cdot}SiO_2$	Tricalcium silicate
Belite	C_2S	$2CaO{\cdot}SiO_2$	Dicalcium silicate
Aluminate	C_3A	$3CaO{\cdot}Al_2O_3$	Tricalcium aluminate
Ferrite	C_4AF	$4CaO{\cdot}\ Al_2O_3{\cdot}Fe_2O_3$	Tetracalcium aluminate ferrite

As alite and belite hydrate, they form different amounts of calcium-silicate-hydrates (C-S-H) and portlandite (CH). The binder obtains most of its properties from C-S-H, that accounts for about 70 wt.% of the hydrated cement paste. CH accounts for about 20 wt.% of the hydrated paste [5]. The remaining hydration phases are mostly aluminium and iron containing phases, such as ettringite. If SCMs are present in the binder, they may react with CH to form additional C-S-H. This is reffered to as a pozzolanic reaction.

1.3. Carbonation of concrete

Carbonation is one of the major deterioration mechanisms for reinforced concrete because it may cause corrosion of the reinforcement steel. Corrosion of the reinforcement is a major threat for the durability and structural integrity of concrete structures, and is the most widespread cause of deterioration for reinforced concrete [6]. Carbonation in concrete is the spontaneous reaction of the alkaline constituents of the concrete with carbon dioxide from the air. Carbonation causes the pH of the pore solution to drop from pH between 13 and 14 in sound concrete, towards neutral values. Steel normally corrodes in contact with oxygen and water, but the high pH environment maintains a passive film around the steel that prevents it from corroding. As the carbonation process lowers the pH, the steel is depassivated, making the reinforcement susceptible for corrosion [7].

As CO_2 is diffusing through the concrete from an exposed surface, it dissolves in the basic pore solution (Equation 2) [6]. The carbonate ions (CO_3^{-2}) then proceed to react with the calcium ions (Ca^{2+}) in the pore solution, forming calcium carbonate crystals ($CaCO_3$) with low solubility (Equation 3) [6]. As more CO_2 enters the concrete, the formation of $CaCO_3$ obtains the necessary OH^- and Ca^{2+} from the dissolution of portlandite ($Ca(OH)_2$) (Equation 4) [6]. This dissolution will continue until all $Ca(OH)_2$ has been dissolved. When all the $Ca(OH)_2$ has been consumed, C-S-H will dissolve subsequently by giving away Ca^{2+} (Equation 5) [6], that reacts further with CO_3^{-2} to form $CaCO_3$ (Equation 3).

$$CO_2 + 2OH^- \rightarrow {CO_3}^{2-} + H_2O \quad (2)$$

$$Ca^{2+} + {CO_3}^{2-} \rightarrow CaCO_3 \quad (3)$$

$$Ca(OH)_2 \rightarrow Ca^{2+} + 2OH^- \quad (4)$$

$$xCaO.SiO_2(aq) + zH_2O \rightarrow yCa^{2+} + 2yOH^- + (x-y)CaO.SiO_2(aq) \quad (5)$$

The rate of carbonation in concrete depends on environmental factors, as well as factors related to the concrete composition. The most relevant environmental factors are humidity, concentration of carbondioxide and temperature. The most relevant concrete composition factors are mainly the alkalinity and permeablilty of the concrete [7].

Diffusion of CO_2 in concrete happens mainly through the air-filled pores. The diffusion rate decreases with increasing humidity and is zero in water-saturated concrete. In dry concrete the carbonation rate is negligible because the carbonation reaction requires water in order to take place. This means that the carbonation rate is slow in both very dry and very wet concrete [7]. In an environment with constant relative humidty and under the conditions of equilibrium, the relationship between relative humidity and carbonation rate can be expressed through the graph in Figure 1 [8]. The graph shows that the most critical environment for facilitating carbonation is an environment with relative humidity about 70%.

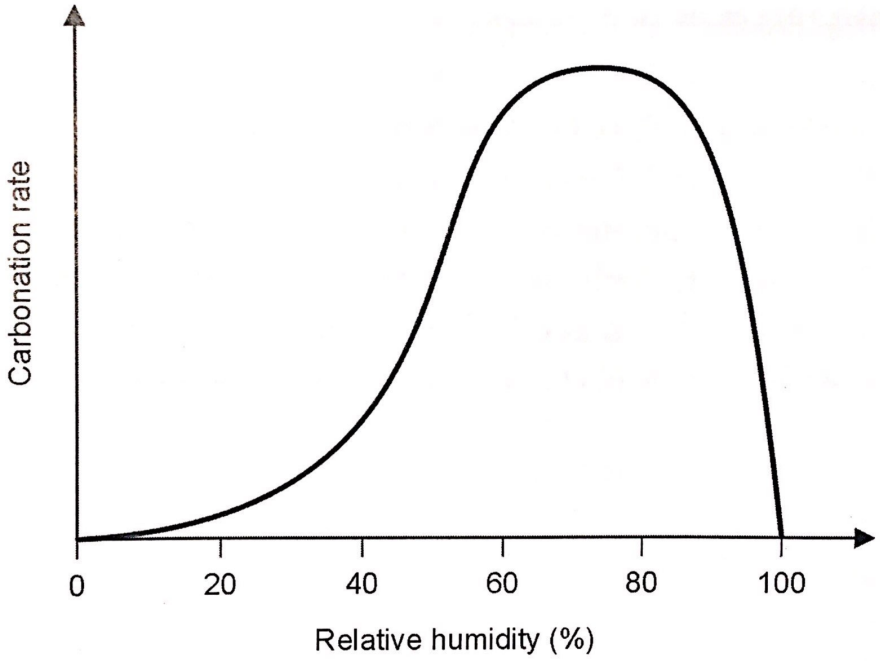

Figure 1 Relationship between relative humidity and carbonation rate in concrete, under equilibrium conditions [8]. Figure borrowed from [7].

If the structure is subjected to periodic wetting, the carbonation rate may be lower than what the relative humidity alone would indicate. The effect of periodic wetting on the carbonation rate depends on wetting time, and the duration and frequency of the wetting-drying cycles [7].

Higher concentration of CO_2 will accelarate the carbonation rate. Normally, the concentration of CO_2 in the atmosphere is about 0.03% in rural areas, and may be up to 0.1% or higher in urban areas [7]. If all other parameters are equal, an increase in temperature will generally lead to an increase in the carbonation rate, as is commonly known for chemical reactions.

Among the factors related to concrete composition that influence the carbonation rate, the permeability has major impact, as it greatly influences the diffusion of CO_2 in the concrete. Limiting the permeability of the concrete may be achieved by lowering the w/c ratio [9]. It is important to properly cure the concrete in order to achieve the advantages of a low w/c ratio, as poor curing leads to the cement matrix being more porous [7].

The carbonation rate is also influenced by the type of cement, specifically, the concrete's capacity to bind CO_2. This capacity is proportional to the alkalinity of the concrete. The capacity to fix CO_2 tends to decrease with increasing amounts of supplementary cementitious materials (SCMs), e.g. ground granulated blast-furnace slag (GGBFS). Blended cements have a lower $Ca(OH)_2$-content because of the clinker replacement and pozzolanic reaction of SCMs [10]. However, blended cements are typically less permeable, and this compensates for being the lower alkalinity and $Ca(OH)_2$-content.

The reinforcement steel is depassivated as the carbonation front reaches it, and will be susceptible for corrosion if oxygen and water is present. A sufficient amount of oxygen to permit corrosion may always reach the surface of the steel, except for conditions where the concrete is completely and permanentely water-saturated [7].

1.4. Research questions

In this report we test the carbonation resistance of a novel low clinker cement with high value industrial by-products introduced in the EnDurCrete project, by comparing its performance to an already comercially available blended cement. We will determine the ingress of the carbonation front under accelerated laboratory conditions (1% CO_2, 60% RH) on both mortar and concrete after 14, 28 and 90 days. We will estimate the carbonation depth using two different techinques: thymolphtalein pH indicator and thermogravimetric analysis (TGA). In addition, we will determine the relative humidity in the samples prior to exposure. This will serve as an important input parameter for a carbonation model, which will be developed by another project partner.

The report aims to answer the following research questions:

- RQ1: Does the EnDurCrete cement lead to a similar or better performance with regards to carbonation resistance compared to the reference cement?
- RQ2: Do the mortar and concrete results agree?
- RQ3: What is the relative humidity in the samples prior to exposure?
- RQ4: Do the different techniques applied to determine the carbonation rate give comparable results?

1.5. Limitations for the project

The carbonation testing associated with this report is limited to samples exposed to accelerated carbonation conditions in the labortatory, not field testing with natural carbonation.
The results from the carbonation testing at NTNU will be used for calibration and verification of a carbonation model for concrete that is being developed within the EnDurCrete project. In this report focus on the experimental verification, and not the carbonation modelling.

Two sets of prisms were prepared, one set with w/c 0.5 and one set with w/c 0.6. After the first measurements of the carbonation depth in the samples using pH indicator thymolphtalein, it appeared that the samples with w/c 0.5 were carbonating very slowly. The carbonation depth would not reach sufficient depth for verification of the model within the time frame of the project. Therefore will only results for the samples with w/c 0.6 be presented in this report.
Additional drying experiments in order to further information in the moisture transport in the samples are being performed by ZAG (project partner in EnDurCrete).

2. Methods

2.1. Materials and mixing proportions

Two different cements were used in this project; CEMII/C-M(S-LL) and CEMII/A-S 42,5 R (here after refered to as CEMII/A-S). The former is the cement developed for the EnDurCrete project, while the latter would be used as a reference cement. The motivation for using these cements was being able to compare the new cement developed within the EnDurCrete project with a benchmark cement that was already comercially available in Europe. The components of the binders are Portland cement (CEMI 52,5R), ground granulated blast-furnace slag (GGBFS) and limestone filler. Both binders were produced in the same cement plant, so that they contain the same type of components, though in different ratios as shown in Table 2.

Table 2: The composition of the CEMII/C-M(S-LL) EnDurCrete binder and CEMII/A-S reference binder.

	CEMII/C-M(S-LL) [wt%]	**CEMII/A-S [wt%]**
CEMI 52,5R	50	83
GGBFS	40	13
Limestone filler	10	4

The components of the two binders were also ground using different grinding procedures. For the CEM II/A-S all the components were co-ground, while the components for the CEM II/C-M(S-LL) were ground separately. Grinding the materials separately allows for better control of the grain size distribution of the binder. Limestone filler is not a reactive component, and does therefore not need to be ground very fine. The reactive components, CEMI 52,5R and GGBFS, should be finely ground to ensure good reactivity. As the limestone filler is a softer material, grinding it together with CEMI 52,5R and GGBFS will cause it to be ground excessively. GGBFS is also usually harder to grind than clinker, therefore can co-grinding of these materials result in too coarse GGBFS and too fine clinker [6]. Grinding the materials separately not only ensures the optimal grain size for all components, it also optimizes the energy used on grinding.

The original concrete mix designs proposed for the project were concretes intended exposed for marine, tunnel or off-shore conditions. Typically these concretes have relatively low w/c-ratios, making them less likely to suffer from carbonation through their lifetime. It was therefore decided that HeidelbergCement would propose a new mix design suitable for a carbonation exposure class (XC). The concrete for the carbonation experiments was based on the concrete for marine conditions, with an increased w/c-ratio. HeidelbergCement proposed a mix design, and Acciona adapted the proposal to produce two sets of concrete prisms, one set with w/c-ratio of 0.5 and one with w/c-ratio 0.6 (Table 3). The notation of the samples are E or R for EnDurCrete or reference cement, 05 or 06 for w/c 0.5 and w/c 0.6, and C or M for concrete or mortar.

Table 3 Concrete mix design for w/c= 0.5 and w/c=0.6 for the EnDurCrete binder CEMII/C-M(S-LL) and the reference binder CEMII/A-S, adapted by Acciona based on the proposal from Heidelberg Cement.

	EDC concrete [kg/m³]	Reference concrete [kg/m³]	EDC concrete [kg/m³]	Reference concrete [kg/m³]
Notation	**E05C***	**R05C***	**E06C**	**R06C**
CEM II / C-M (S-LL)	350	-	315	-
CEM II / A-S	-	350	-	315
Washed sand 0/4	49	49	51	51
Gravel Pisello 5/10	16	16	12	12
Gravel 10/15	35	35	38	38
VC-2014 (60%) / VF-10150666 (40%)	3.3	5.3	1.1	2.0
w/c ratio (target)	0.5	0.5	0.6	0.6
w/c ratio (effective)	0.5	0.5	0.6	0.6

*Note that as mentioned in 1.5, that the w/c 0.5 samples will not be used further in the study.

In addition to concrete samples, mortar samples were also prepared. Possible solutions for designing concrete equivalent mortar samples from the concrete design mix were discussed at several project meetings. It was decided that concrete equivalent mortar samples would be achieved by preparing the mortar with the same dosages as for concrete, except the gravel. The water content was decreased to account for the water that normally would be absorbed by the coarse gravel in the concrete. This would give samples with similar water to cement ratio, the same grain size between mortar and mortar in the concrete and similar interfacial transition zone. The mortar mix design is given in Table 4.

Table 4 Mortar mix design for w/c= 0.5 and w/c=0.6 for the EnDurCrete binder CEMII/C-M(S-LL) and the reference binder CEMII/A-S, adapted by Acciona

	EDC mortar [kg/m³]	Reference mortar [kg/m³]	EDC mortar [kg/m³]	Reference mortar [kg/m³]
Notation	**E05M***	**R05M***	**E06M**	**R06M**
CEM II / C-M (S-LL)	552	-	487	-
CEM II / A-S	-	552	-	487
Washed sand 0/4	100	100	100	100
Gravel Pisello 5/10	-	-	-	-
Gravel 10/15	-	-	-	-
VC-2014 (60%) / VF-10150666 (40%)	3.2	3.9	1.4	1.7
w/c ratio (target)	0.5	0.5	0.6	0.6
w/c ratio (effective)	0.48	0.48	0.58	0.58

*Note that as mentioned in 1.5, that the w/c 0.5 samples will not be used further in the study.

2.2. Casting and curing of samples

Prims of 10x10x40 cm were cast by Acciona according to EN 12390-2 [11], for both concrete and mortar samples. For the experiments performed at NTNU, 3 concrete prisms and 4 mortar prisms were cast for each of the different binders, and each of the different w/c ratios. This summed up to 28 prisms in total. Extra mortar samples were needed for additional testing that would be performed only on mortar.

After demoulding the samples after 1 day, they were cured wrapped in plastic in a >95% RH humidity chamber at 20 °C until 28 days old. After 28 days of curing, the concrete and mortar prisms were sent from Acciona to NTNU. The prisms were double wrapped in several layers of plastic during shipping to avoid drying and carbonation. Upon arrival at NTNU the prisms were kept in the packaging in a temperature-controlled room at 20 °C until exposure.

2.3. Exposure

The concrete prisms were sawn into four blocks of 10x10x7 cm, while the ends of the prisms were discarded (Figure 2). The sides of the blocks were assigned a letter from A-D, where A and C were sawn surfaces (Figure 2). After sawing the prisms into blocks they were placed in a carbonation chamber holding 20 °C, 60% RH and 1% CO_2. This exposure was chosen in order to accelerate the carbonation process. The blocks were placed in the carbonation chamber with the sawn surfaces approximately 7 cm apart to ensure good air flow between the blocks as shown in Figure 3. The blocks were exposed for 14, 28 and 90 days.

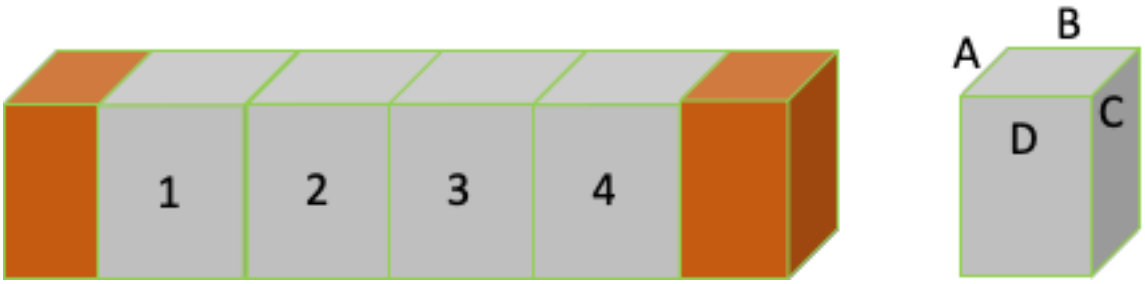

Figure 2 Illustration of conrete/mortar prism divided in four blocks for exposure in carbonation chamber. The ends (orange) were discarded. The sides of each block were assigned a letter A-D. A and C were sawn sufaces.

Figure 3 Sawn blocks ready for exposure in the carbonation chamber.

2.4. Carbonation depth measurements with pH indicator

After 14, 28 and 90 days of exposure the sample blocks were split in the center and immediately sprayed with pH indicator, 1 % thymolphtalein solution. The solution was prepared by dissolving 1 g of the indicator in 20 ml of deionized water and 70 ml of ethanol. Thymolphtalein has a blue/purple colour when the pH is higher than 9-10.5 [12], and is colourless for pH lower than this.

The carbonation depth of a sample is here defined as the distance perpendicular from the exposed surface to the region coloured by the pH indicator. The non-carbonated parts of the sample are coloured blue due to the high pH in sound concrete. The blocks were split perpendicular to the sawn surface so that the carbonation depth could be measured from the sawn surfaces, and split vertically so that the variation in carbonation depth along the height of the block could be studied. The geometry of the split is shown in Figure 4.

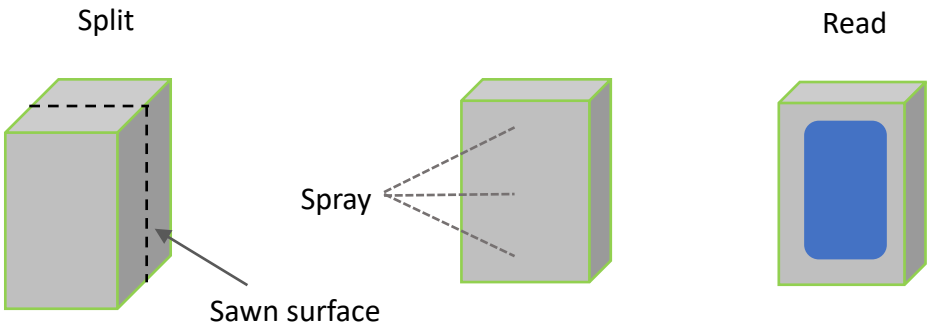

Figure 4 Split geometry for the sample blocks after exposure and spraying of pH indicator.

The carbonation depth was measured by using a measuring rod to measure the distance from the edge of the sample block to the blue non-carbonated area. The measurements were performed according to procedure given in EN 13295 [13]. 5 measurements were taken from each side of the sample block, not including the rounded corners of the non-carbonated area. The measurements were rounded to the closest half millimeter. For measurements where the carbonation front was disturbed by dense aggregates that were unstained by the pH indicator, the measurement was taken by making a theoretical line for the carbonation front through the aggregates. If some measurements were influenced by excessive carbonation along the aggregates, the measurements were discarded. An illustration of this is shown in Figure 5. For each side of the sample block the 5 measurements were used to calculate the average carbonation depth for the given side. The average carbonation depth of each sample specimen was calculated by taking the average value for each of the four sides. Figure 6 shows an actual concrete sample sprayed with thymolphtalein solution.

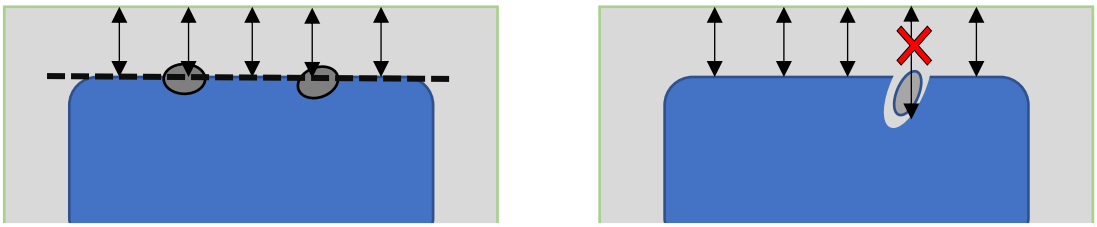

Figure 5 Left: Measuring of carbonation depth when the carbontation front is disturbed by dense aggregates. Right: Measuring of the carbonation depth when carbonation front is influenced by excessive carbonation due to ingress along aggregates. Illustration: (Bjørndal, 2019)

Figure 6 Example of cracked concrete sample sprayed with thymolphtalein solution (left) and detail of the carbonation front (right). Illustration: (Bjørndal, 2019)

The carbonation depth over a sample cross section was expected to vary through the cross section. This variation was expected due to gravity pulling the aggregates in the fresh concrete towards the bottom of the formwork. This makes the top of the sample less dense than the bottom of the sample, making the top parts more prone to suffer from carbonation (Figure 7). Similar results were found by Revert [14]. Other variations in carbonation depth can be caused by inhomogenities in the sample.

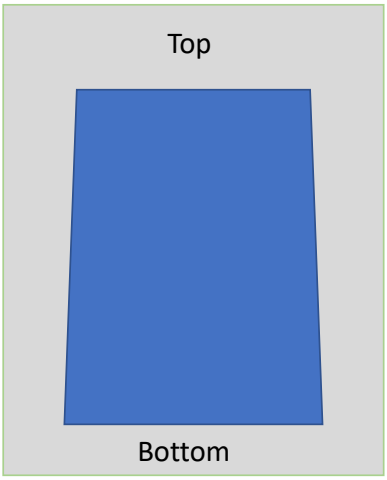

Figure 7 Illustration of the variation in carbonation depths along the top and bottom of a sample's cross section.

All the samples were photographed with a scale after being split and sprayed with thymolphtalein solution. This allows for further study of the carbonation depth using image analysis later.

2.5. Profile grinding and thermogravimetric analysis (TGA)

The thermogravimetric curve (TG-curve) shows the relationship between the temperature in the oven and the sample weight. The different phases in the TGA sample may be identified by studying the first derivative of the TG-curve (DTG-curve). Different phases decompose at different temperatures, and the corresponding mass

loss results in peaks in the DTG-curve. In order to detect the different phases, the DTG-curves can be divided into several temperature intervals as suggested by Lothenbach et al.[15]. The first peak appears at about 100 °C, as ettringite decomposes and dehydroxylation of C-S-H starts. C-S-H gradually decomposes as the temperature increases from 50 °C to 600 °C. The decomposition of portlandite takes place between 400 °C and 500 °C. Carbonate decomposes at temperatures higher than 600 °C. An example of the different peaks is shown in Figure 8 [15].

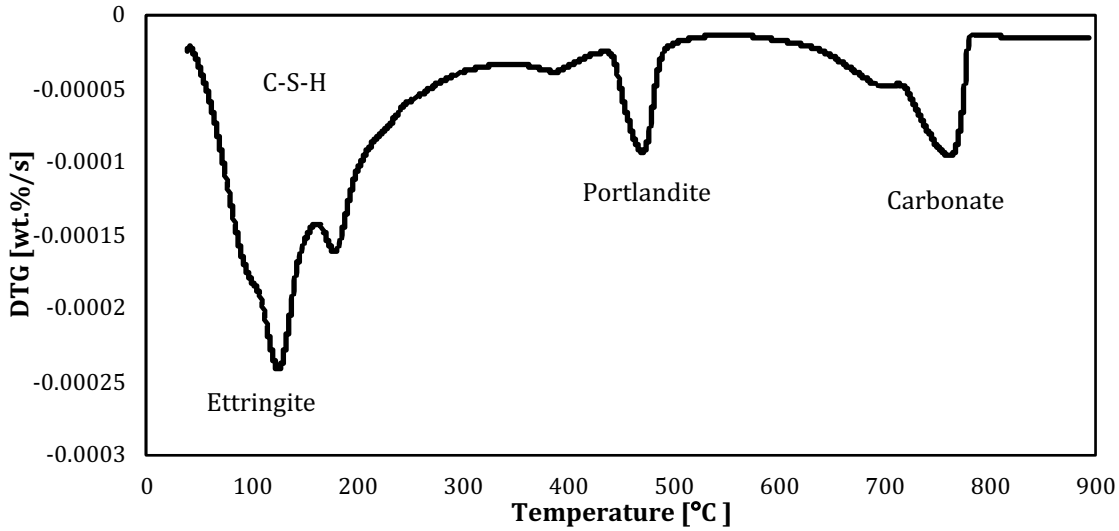

Figure 8 Example of peaks in DTG-curve in a pure paste sample, adapted from Lothenbach et al. [15].

TGA may also be used to quantify the amounts of bound water in the sample. This can be obtained by measuring the mass loss in the sample from starting temperature at 40 °C up to 500 °C or 550 °C. This can be done because all mass loss occuring below 600 °C is caused by the release of water. Decomposition reactions from 600 °C to 900 °C emit CO_2. Mass loss for the temperature interval 600-900 °C is an indication that the sample is carbonated. The DTG-curve for a carbonated sample will show a small or no portlandite peak, and a deeper carbonate peak compared to the DTG-curve in Figure 8.

Profile grinding was performed only on mortar samples. The grinding was performed from a sawn surface (side A) in predetermined steps, as shown in Figure 9. The carbonated sides of the sample was discarded in order to obtain 1D carbonation profiles. The grinding steps for the profile grinding were determined by the approximate location of the carbonation front obtained by the carbonation depth measurments with pH indicator. In the range of the carbonation front the samples were ground in steps of 1 mm, the remaining parts of the samples was ground in 2 mm steps. The TGA was performed using a Mettler Toledo TGA/DSC 3+, on homogenized samples of approximately 300 mg placed in aluminium oxide cruicibles. At a rate of 10°C/min the samples were heated from 40°C to 900°C while the oven was purged with 50 ml/min N_2. The sample mass was monitored as a function of the temperature. The phase changes upon carbonation were identified by comparing the DTG-curves.

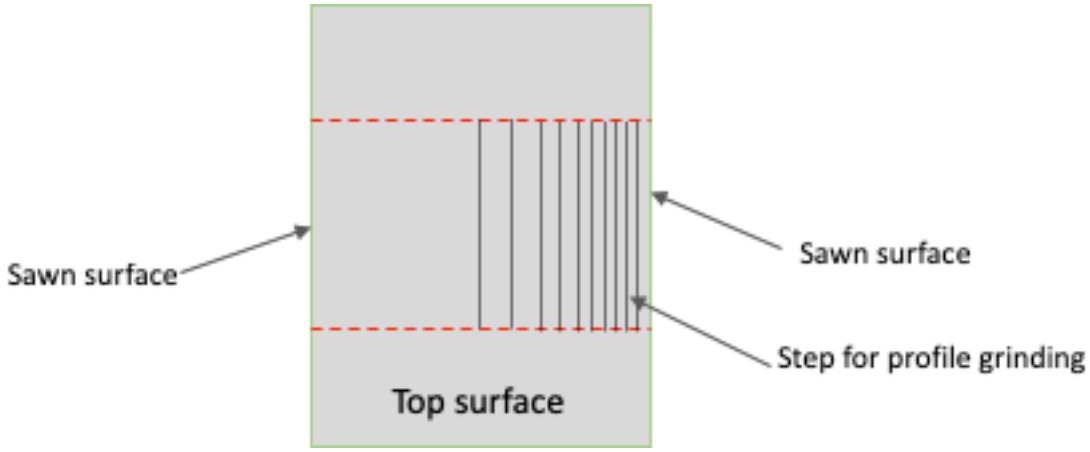

Figure 9 Illustration of profile grinding steps, from a sawn surface. Parts outside the dashed lines were discarded in order to obtain 1D carbonation profiles.

To quantify the bound water (BW) content equation (6) was applied. The mass losses are expressed relative to the mass at 900 °C ($W_{900\,°C}$), as this remains constantly independent of the carbonation. Sample mass at 50 °C, 400 °C and 500 °C is expressed as $W_{50\,°C}$, $W_{400\,°C}$ and $W_{500\,°C}$. The mass at different temperatures is given in % per sample weight, to make it easier to compare the results from different samples. The weight loss from 50 °C to 900 °C and from 50 °C to 550 °C were determined by horizontal steps along the temperature axis. The amount of portlandite (CH) quantified using equation (7). The weight loss from 400 °C to 550 °C was determined by integrating the DTG-curve between approximately 400 °C and 550 °C with a linear base line. 74/18 represents the ratio between the molar weight of portlandite (74 g/mol) and the molar weight of water (18 g/mol). By using this method one obtains similar results as using tangential step, and the weight loss from decomposition of C-S-H is excluded [9].

$$BW\ \% = \frac{W_{50°C} - W_{550°C}}{W_{900°C}} \cdot 100\% \qquad (6)$$

$$CH\ \% = \frac{W_{400°C} - W_{550°C}}{W_{900°C}} \cdot \frac{74}{18} \cdot 100\% \qquad (7)$$

2.6. Relative humidity measurements of crushed samples

In order to obtain information on moisture transport in the samples, it was originally planned to condition the concrete and mortar samples to RH=60% before resaturating and then stepwise drying them. This preconditioning would last for weeks, possibly months, and we would not obtain the required results within the time frame of the project. This was therefore discarded by the project group. In order to obtain information on the relative humidity (RH) of the samples at a starting point before carbonation, the relative humidity was measured when the samples were removed from sealed state. The measurements were performed on a separate prism, to make

sure that the humidity state that was tested would be representable for the the other samples.

The humidity sensors used were Vaisala HMP44 probes with Vaisala HMI41 indicator (Figure 10). The accuracy of the probes is ±2% RH for up to 90% RH, and ±3% RH for 90-100% RH. The sensors were calibrated by SINTEF Community approximately 4 weeks before the measurements. The calibration was performed at 20 °C, for 75%, 80%, 85%, 90% and 95% RH. During the calibration the HMP44 sensors were placed in the Rotronic Hygrogen2 humidity generator together with the probe from the MBW 473-RP2 Dew point mirror, as shown in Figure 10. The Rotronic Hygrogen2 created a stable reference environment with the desired temperature and RH. Using the MBW 473-RP2 Dew point mirror during the calibration provided a precise measurement of the actual RH in the humidity generator. For each of the RH steps the measured temperature and RH for each of the HMP44 sensors were read using the HMI41 indicator. The sensors were calibrated again after the measurements were finished. The calibration was performed to make sure that the sensors were working correctly before and after the measurements, and the calibration results for each sensor were used to calculate the actual value for the relative humidity. The sensors were aired out several days before starting the measurements to avoid residual moisture from the calibration which would give incorrect measurements.

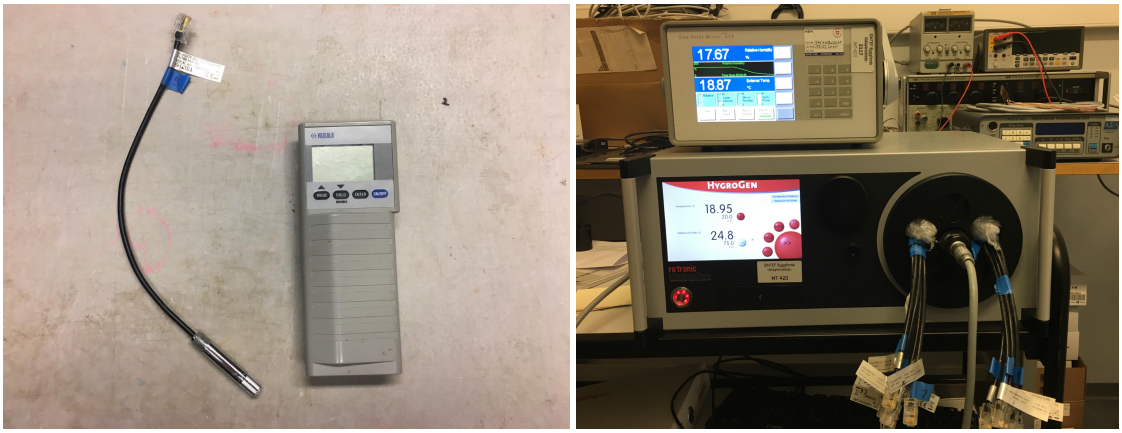

Figure 10 Left: HMP44 temperature and humidity probe and HMI41 indicator. Right: Calibration setup: MBW 473-RP2 (top) and Rotronic Hygrogen2(bottom) with the HMP44 sensors and the dew point mirror hygrometer probe from the MBW 773-RP2 (grey wire) inserted.

The concrete and mortar samples were removed from the packaging and split into smaller sub-samples. The outer 2-3 cm of the sub-samples were split of. The remaining inner parts of the sub-samples were crushed with a hammer on a metal plate. Pictures of the equipment used for breaking and crushing the concrete and mortar prisms are shown in Figure 11. To prevent drying, one person crushed the sub-sample and one person gathered pieces of the sub-sample into glass tubes. For concrete samples pieces containing mostly aggregates were discarded. All parts of the sample that were not worked on were immediately wrapped in plastic and kept sealed at all times. The glass tubes were filled 2/3 with mortar or concrete pieces of approximate size 5 mm and sealed using rubber stoppers. Glass tubes with 18 mm inner diameter were chosen in order to have a sufficient amount of material for the measurements. The glass tubes were then placed in a climate chamber at 50% RH and 20 °C for at least 30 minutes before installing the sensors. This allowed the samples to

approach thermal equilibrium with the surrounding environment, and by that avoid condesation in the tubes disturbing the measurements.

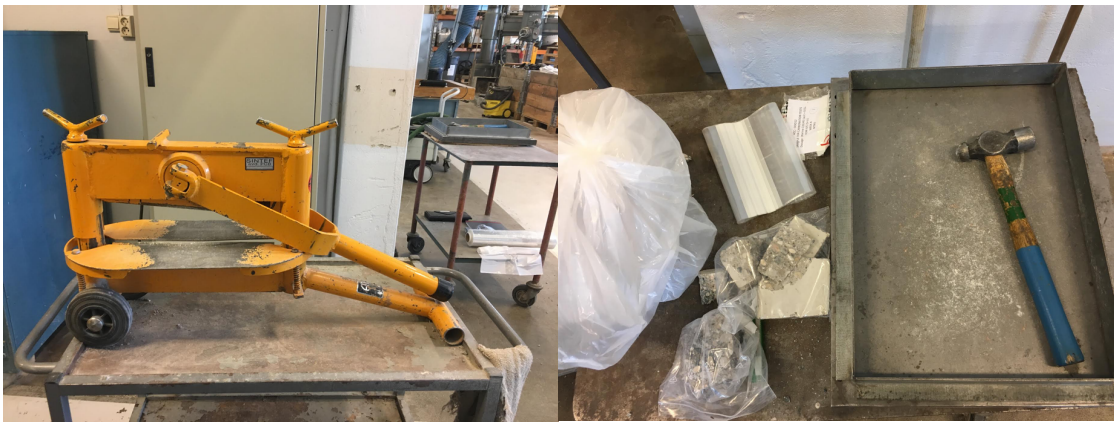

Figure 11 Equipment for breaking the concrete and mortar prisms. Left: sample splitter. Right: Plastic bags, metal plate and frame, and hammer.

The humidity sensors were placed in the glass tubes with cut stoppers and sealed with two layers of parafilm (Figure 12). The glass tubes contained as many pieces as possible without any sample material being in contact with the sensors. The glass tubes were placed in an insulated holder during the measurment period as shown in Figure 12. The relative humidity in the glass tubes was measured for the first time approximately 24 hours after the sensors were placed and measured every morning for following 4 days. The measurements were performed in the morning to take advantage of the climate chamber being closed, leaving the samples undisturbed in stable temperature during the night.

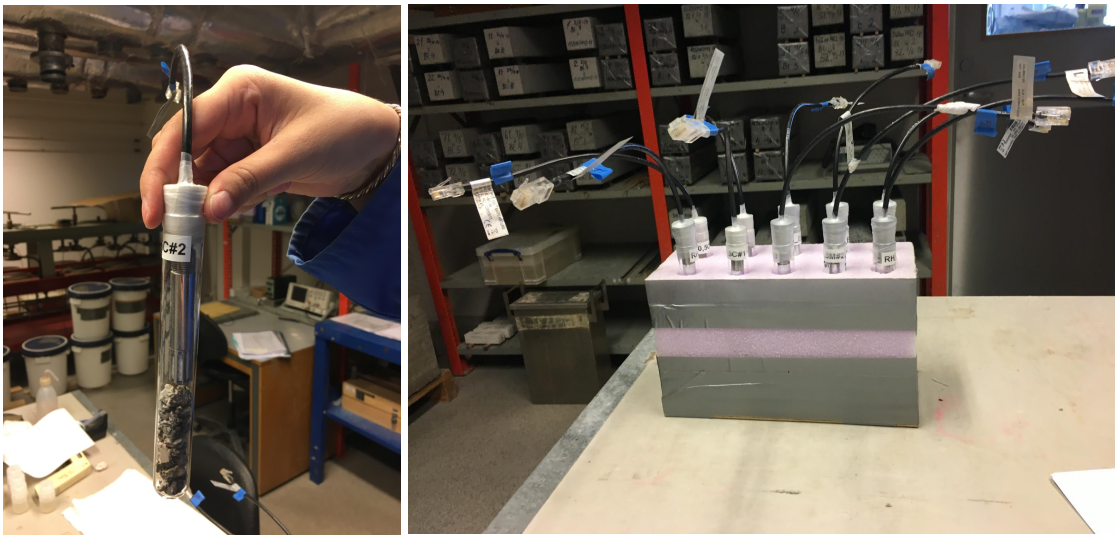

Figure 12 Left: glass tube with sample pieces and humidity sensor, sealed with parafilm. Right: glass tubes in the insulated holder.

The results from the calibration of the sensors showing the relationship between the measured and the actual RH, were used to correct the values measured in the samples. For samples that have been prepared without being dried excessively, the RH was expected to increase during day 1, and then stabilize during day 2 and 3. The final value for the RH of each sample was calculated by averaging the measurements from day 2-4. As the sample prisms were sealed since casting, high RH was expected.

3. Results

3.1. Carbonation depth with pH indicator

The measured carbonation depth for EnDurCrete mortar sample with w/c 0.6 (E06M1) shows greater carbonation depth for the top of the sample, and smaller depth for the bottom of the sample after 90 days of exposure (Figure 13). The carbonation depth along side A and side C is between the top and bottom values. This is as observed by Revert et al. [14], who used a similar method. However, it is not the case for all samples. Some samples show greater carbonation depth at the bottom and sides, than at the top.

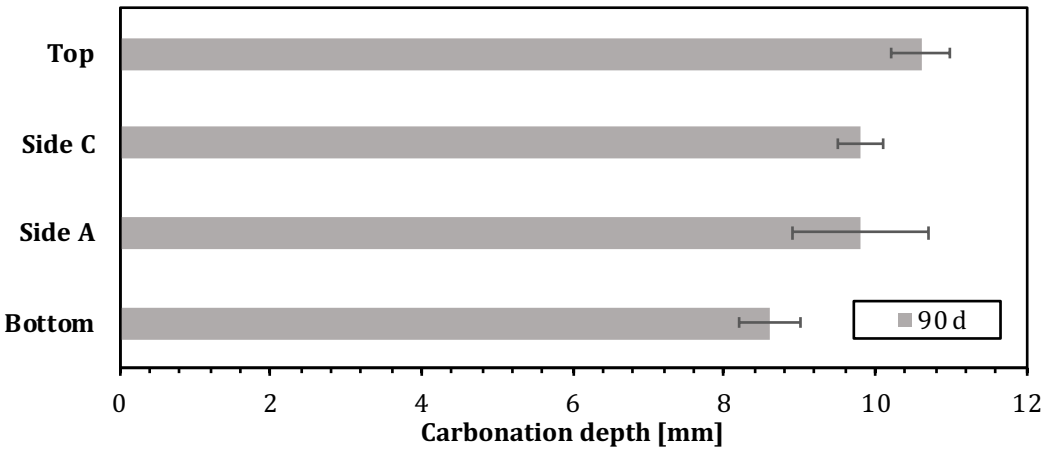

Figure 13 Variation in carbonation depths over different sides of the sample E06M1. The carbonation depth is the largest for the top and smallest for the bottom of the sample.

The development of carbonation depth over time is presented for side A only, as side A was the side profile ground for TGA. Remaining results may be found in Appendix A. As shown in Figure 14, the carbonation depths for both the EnDurCrete and the reference mortar increase over the exposure time. The reference mortar has lower carbonation depth than the EnDurCrete mortar at all times, and the difference between them increases over time.

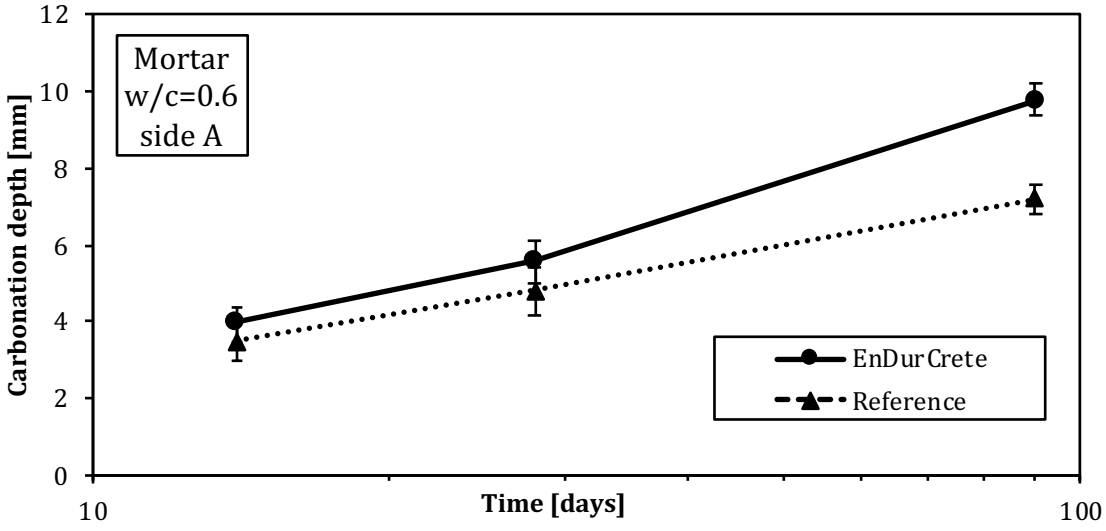

Figure 14 Carbonation depths over time for EnDurCrete and reference mortar, side A

In the case of concrete, the carbonation depth also increases over time for both the EnDurCrete and the reference concrete, as shown in Figure 15. The carbonation

depths for the two concretes are quite similiar for the entire exposure time. When the standard deviations for the measurements are taken into account the measurements are overlapping with each other at all three measurement dates.

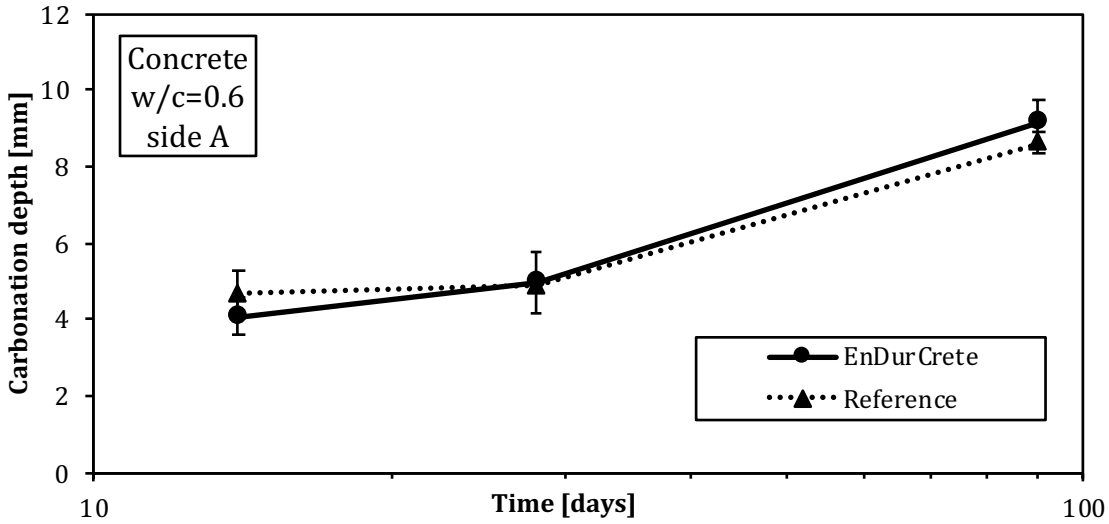

Figure 15 Carbonation depth over time for EnDurCrete and reference concrete samples, side A

3.2. Thermogravimetric analysis (TGA)

Figure 16 and Figure 17 show examples of TG- and DTG-curves for the EnDurCrete mortar sample after 28 days of exposure. Carbonated grindig steps are indicated with dashed lines. The DTG-curves for the non-carbonated steps show a small portlandite peak just below 500 °C, while the carbonated steps do not have this peak (Figure 17). The carbonate peak is also slightly deeper for the carbonated samples than for the non-carbonated samples. Note that the non-carbonated sections show a large carbonate peak as they contain 10 % limestone (mainly $CaCO_3$).

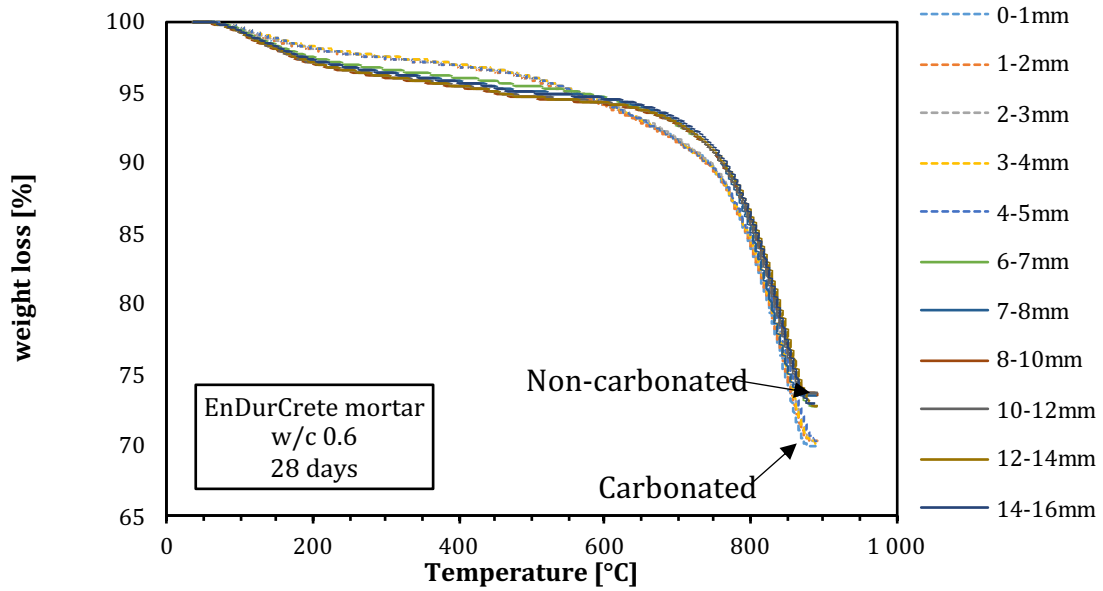

Figure 16 TG-curves for EnDurCrete sample with w/c 0.6 after 28 days of exposure. Dashed lines indicate carbonated grinding steps.

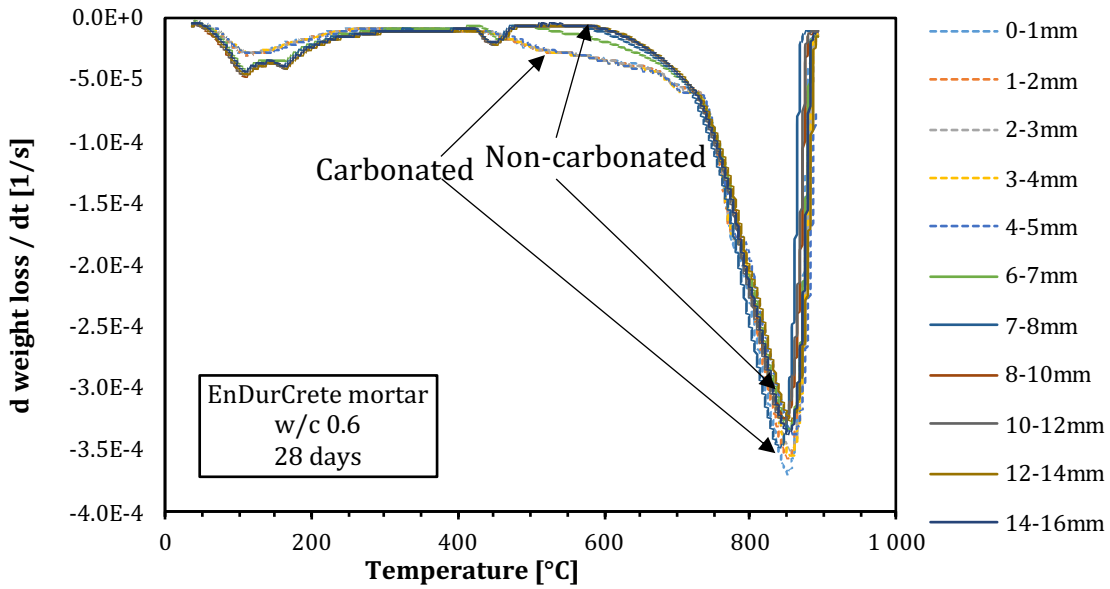

Figure 17 DTG-curves for for EnDurCrete sample with w/c 0.6 after 28 days of exposure. Dashed lines indicate carbonated grinding steps.

Figure 18 shows the portlandite content (a) and bound water content (b) for the EnDurCrete mortar after 14, 28 ans 90 days of exposure. For all exposure dates the portlandite content at the exposed surface is zero, and over the depth of the sample increases to reach a plateau. The depth where there is no portlandite present increases over time. The bound water content is related to the presence of hydration products, and indicates that the amount of hydration products in the sample change over the depth of the sample. The bound water content is higher in the non-carbonated steps of the samples. For the 90 days exposure the relative bound water content is lower than for 14 and 28 days. The change in bound water agree well with the change in portlandite for the corresponding exposure dates. The sample for 90 days exposure should have been profile ground a few millimeters deeper in order to make sure that a plateau was obtained for both portlandite and bound water.

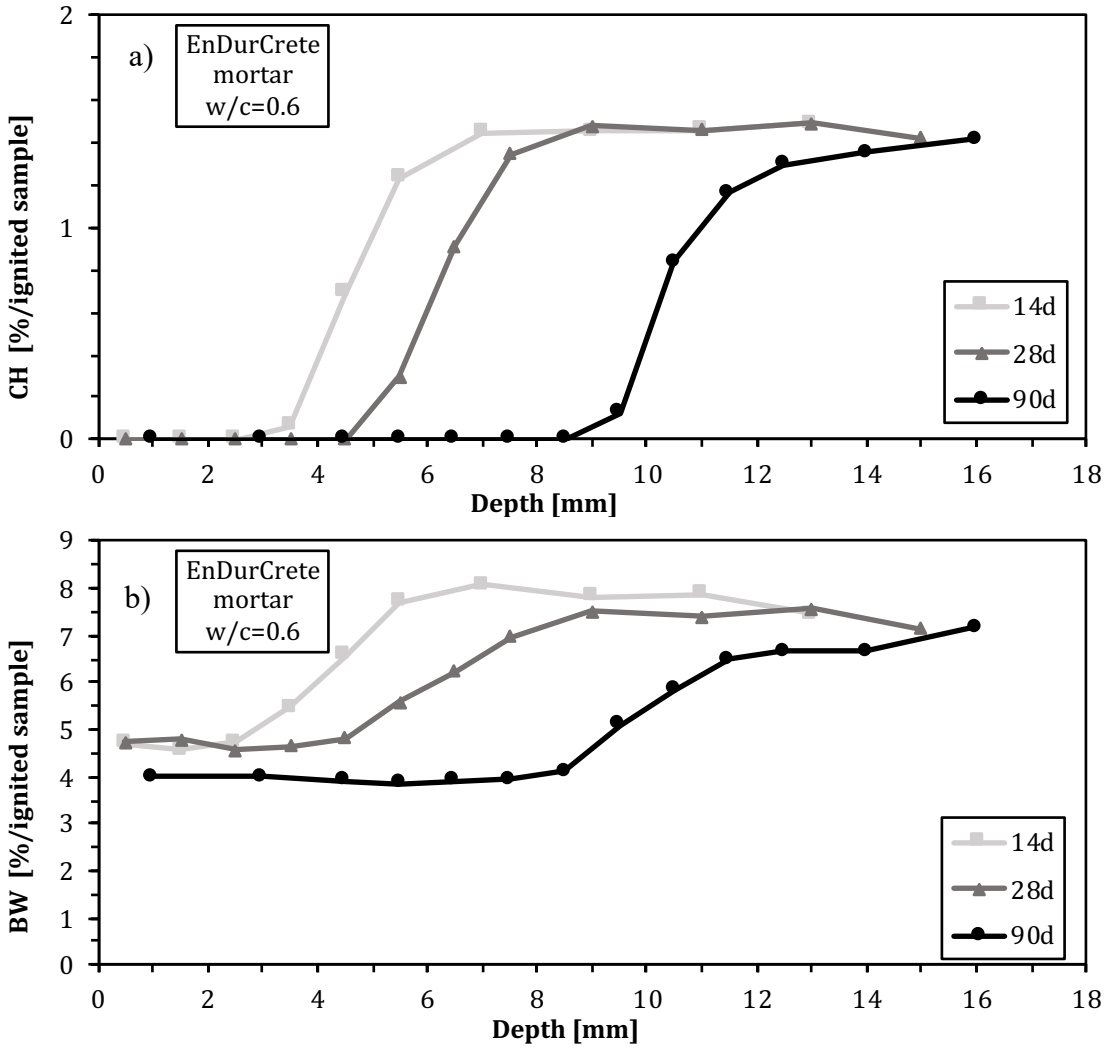

Figure 18 a) Portlandite (CH) content and b) bound water content in EnDurCrete samples after 14 days (square), 28 days (triangle) and 90 days (circle).

Figure 19 shows the portlandite (CH) content (a) and bound water content (b) for the reference mortar after 14, 28 ans 90 days of exposure. In Figure 19 a) the depth where the portlandite content is zero increases over the exposure time. All three exposure dates reach approximately the same portlandite content. For the bound water content (Figure 19 b) changes over the depth of the sample, and change agrees well with the change in portlandite content. The bound water content is higher in the non-carbonated steps of the samples. The bound water content for the 90 days exposure sample is lower than for the 14 days and 28 days. The 90 days of exposure sample does not have a should have been profile ground a few millimeters deeper in order to obtain a plateau level.

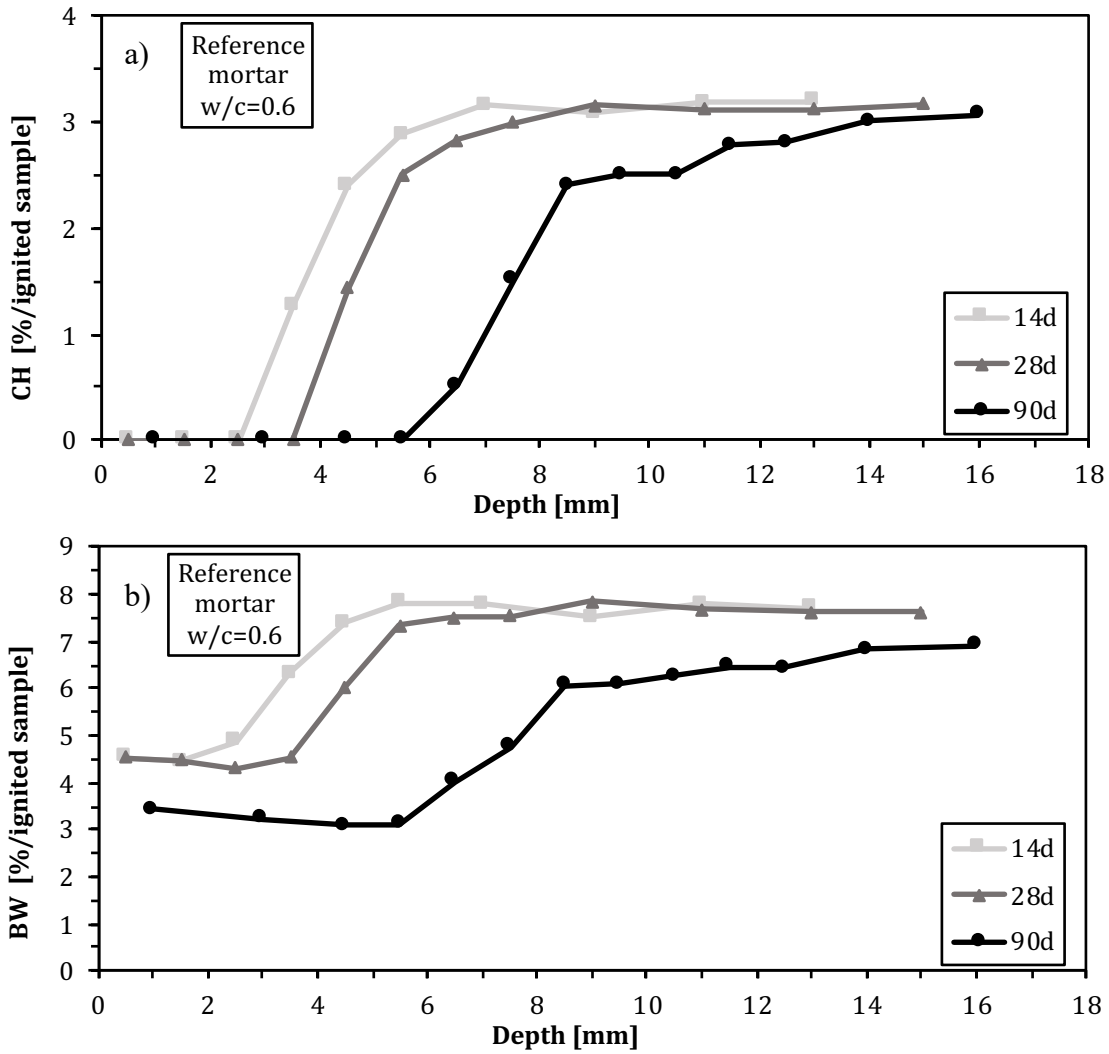

Figure 19 a) Portlandite (CH content) and b) bound water content in reference samples after 14 days (square), 28 days (triangle) and 90 days (circle).

3.3. Relative humidity measurements

An example of the calibration results for one humidity sensor is presented in Figure 20. The value for R^2 is 1 and indicates that linear trend line fits well. This suggests that the sensor works properly and can provide reliable results. All measurements performed during the measurement period are corrected using the equation of the linear trend line for the corresponding humidity sensor. All measurements, calibration results and curves, and the corrected values may be found in Appendix B.

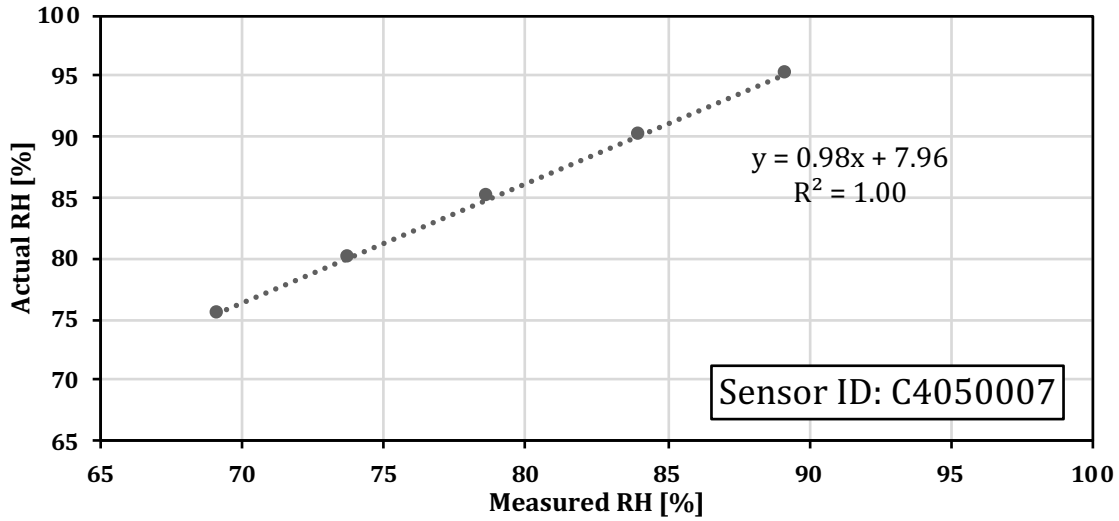

Figure 20 Example of calibration results used to find the relationship between the measured RH and the actual RH for sensor C4050007.

The average value and the standard deviation of the relative humidity measured over day 2, day 3 and day 4, as well as the average relative humidity for mortar and concrete is presented in Table 5. All average RH values are higher than 88 % RH. For the EnDurCrete binder the average RH is 0.7 % RH higher for the mortar compared to the concrete. For the reference binder the mortar is 0.5 % RH higher than the concrete. These differences are smaller than the corresponding standard deviation for the mortar samples. The average RH and mortar standard deviation are displayed in a bar diagram in Figure 21.

Table 5 Average relative humidity for each sample with w/c=0.6 and average relative humidity for all 10 samples that were measured; 3 EnDurCrete mortar samples, 2 EnDurCrete concrete samples, 3 reference mortar samples and 2 reference concrete samples.

Sensor ID	Sample name	RH [%]	St.dev for each sample	Average RH[%]	St.dev for mortar
C4050007	RH_E0.6M#1	87.8	<0.1		
C3950019	RH_E0.6M#2	89.8	<0.1	89.1	1.1
C4050002	RH_E0.6M#3	89.8	0.1		
C4050001	RH_E0.6C#1	87.1	0.1		
C4050004	RH_E0.6C#2	89.6	0.1	88.4	
E150002	RH_R0.6M#1	91.0	0.4		
G262000 2	RH_R0.6M#2	92.2	0.1	91.8	0.8
F3340019	RH_R0.6M#3	92.0	0.1		
E4330005	RH_R0.6C#1	91.4	0.1		
C3950015	RH_R0.6C#2	91.3	0.1	91.3	

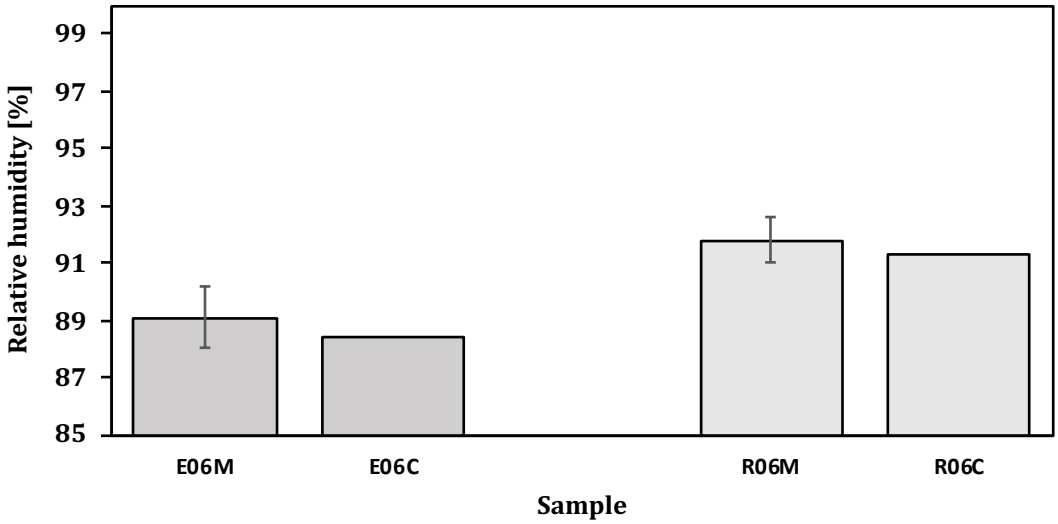

Figure 21 Final results of relative humidity measurements displayed in a bar diagram. EnDurCrete mortar and concrete (left) are dark grey, reference mortar and concrete (right) are light grey. For mortar samples standard deviation bars are included.

4. Discussion

4.1. TGA

The curves for the portlandite content (CH) over the depth of the sample are similar in shape for the EnDurCrete and reference mortar samples, but the relative content of CH is much higher in the reference sample (Figure 22). This agrees well with findings by Leemann et al. [16], where GGBFS containing mortars had a lower CH content due to lower clinker content and additional formation of C-S-H from the hydraulic and pozzolanic reaction of the GGBFS. The reference binder also contains GGBFS, but only 13 wt% compared to the 40 wt% GGBFS in the EnDurCrete binder. It is relevant to note the difference in CH content, as the CH content often is linked to carbonation resistance as it partakes in the carbonation reactions described in 1.3.

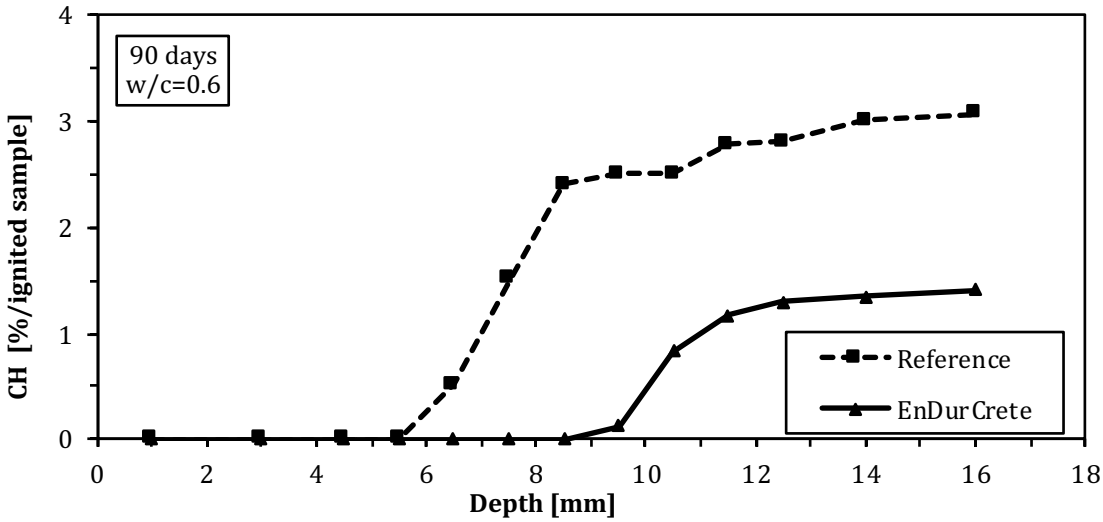

Figure 22 Comparison of relative CH content over the depth of the sample in EnDurCrete (solid line) and reference mortar samples with w/c 0.6.

As mentioned in section 3.2, the bound water content for 90 days exposure is lower over the sample depth than for 14 days and 28 days, for both the EnDurCrete and the reference sample. We have not looked further into this in this study, but one should look further into this in a following study.

4.2. Carbonation depth with pH indicator

For concrete samples the carbonation depths of the EnDurCrete and the reference samples are similar for all measurements. For the mortar samples, the reference cement samples showed less carbonation depth than the EnDurCrete binder samples. All results for mortar and concrete are displayed toghether in Figure 23. The EnDurCrete concrete and EnDurCrete mortar follow each other closely over the entire exposure time. For the reference mortar and reference concrete the carbonation depht is very similar at 28 days of exposure, while at 14 days and 90 days the concrete has a significantly larger carbonation depth than the mortar.

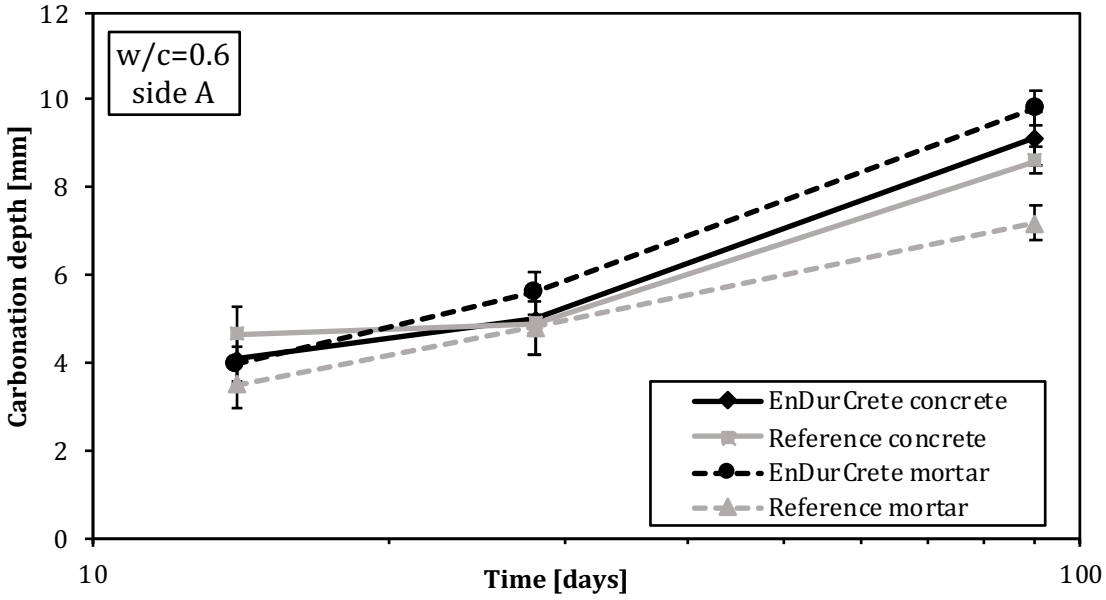

Figure 23 All carbonation depth results for both concrete (solid lines) and mortar (dashed lines) for both EnDurCrete (black) and reference (grey) cements.

The properties of concrete is affected by the disruption in the packing of the cement grains in the bulk paste close to an aggregate. The result is that the region close to the aggregates contains mostly small grains and has a higher porosity. This region is called the interfacial transition zone (ITZ) [17]. The ITZ tends to be more predominant for mix compositions with higher w/c ratios [9], making it possible that the ITZ affects the properties of the mixes with w/c 0.6 that is used in this project. As explained in 1.3, diffusion of CO_2, and thus carbonation, increases when the permeability of the concrete increases. An increase in ITZ diffusivity and thickness might therefore lead to an increase in carbonation [18].

However, a study by Elsharief et al. [19] found no specific trend between the ITZ thickness and aggregate size. Han. et al. [18] also found that the aggregate size had a neligible influence on the carbonation process due to the aggregate volume fraction being constant. The difference in aggregate size or ITZ do therefore not seem to explain the difference in performance between the mortar and concrete with reference cement.

In a study by Han et al. [18] where the carbonation resistance of concretes with different amounts of GGBFS (0%, 30%, 50%, 70%). The study found that the concrete with 70% GGBFS carbonated much faster and the concrete with 0% GGBFS carbonated the slowest. However the concretes with 30% and 50% GGBFS showed a more similar degree of carbonation, with the 50% GGBFS carbonating slightly more. This study shows that higher content of GGBFS may cause an increase in carbonation depth. Nevertheless, this does not explain why the EnDurCrete mortar is carbonated only slightly deeper than the EnDurCrete concrete, while the reference mortar is carbonated significantly less than the reference concrete.

One weakness with the method is that there is only up to 5 measurements for each side of the sample. The carbonation front in the concrete samples is a lot more uneven than for the mortar samples (Figure 24). Presence of aggregates that caused excessive carbonation in the concrete led to up to two out of five measurements for each side of

the concrete samples to be discarded. In order to make sure that the differences in carbonation depths that we observe are genuine, the samples should be studied with more measuring points using image analysis.

Figure 24 Left: carbonation front in mortar sample. Right: carbonation front in concrete sample.

As mentioned in 3.1 the expected larger carbonation depth in the top than the bottom of the samples was not the case for all the samples. The reason for this has not been examined further in this report.

4.3. Comparison of TGA and pH indicator

Phenolphtalein was commonly used as pH indicator for carbonation depth measurements, but has been replaced by thymolphtalein because it has been classified as suspected of causing genetic defects and being carcinogenic [20]. The colour change in phenolphtalein is between pH 8-9.8, and thymolphtalein changes at pH 9-10.5 [12]. The higher range for the colour change would lead to larger carbonation depths for phenolphtalein than for thymolphtalein, if there is a gradual transition between carbonated and non-carbonated parts of the sample. However, by studying the carbonation front by optical microscopy as done by Revert et al. [14], it is clear that the transition zone with the corresponding drop in pH is very narrow. The carbonation depth indicated by thymolphtalein and phenolphtalein should therefore be very similar.

When measuring carbonation depth using pH indicator, the carbonated concrete is the part of the sample that show no change in colour from the indicator. For TGA the carbonation depth is characterized by the decrease in portlandite. The results for carbonation depth using thymolphtalein pH indicator and carbonation depth by TGA are compared in Figure 25, Figure 26 and Figure 27 below. By defining the carbonation depth for the TGA results as the entire depth where the portlandite content is zero, it is clear that the carbonation depth measured using pH indicator is greater for both the EnDurCrete and the reference cement, for all exposure dates.

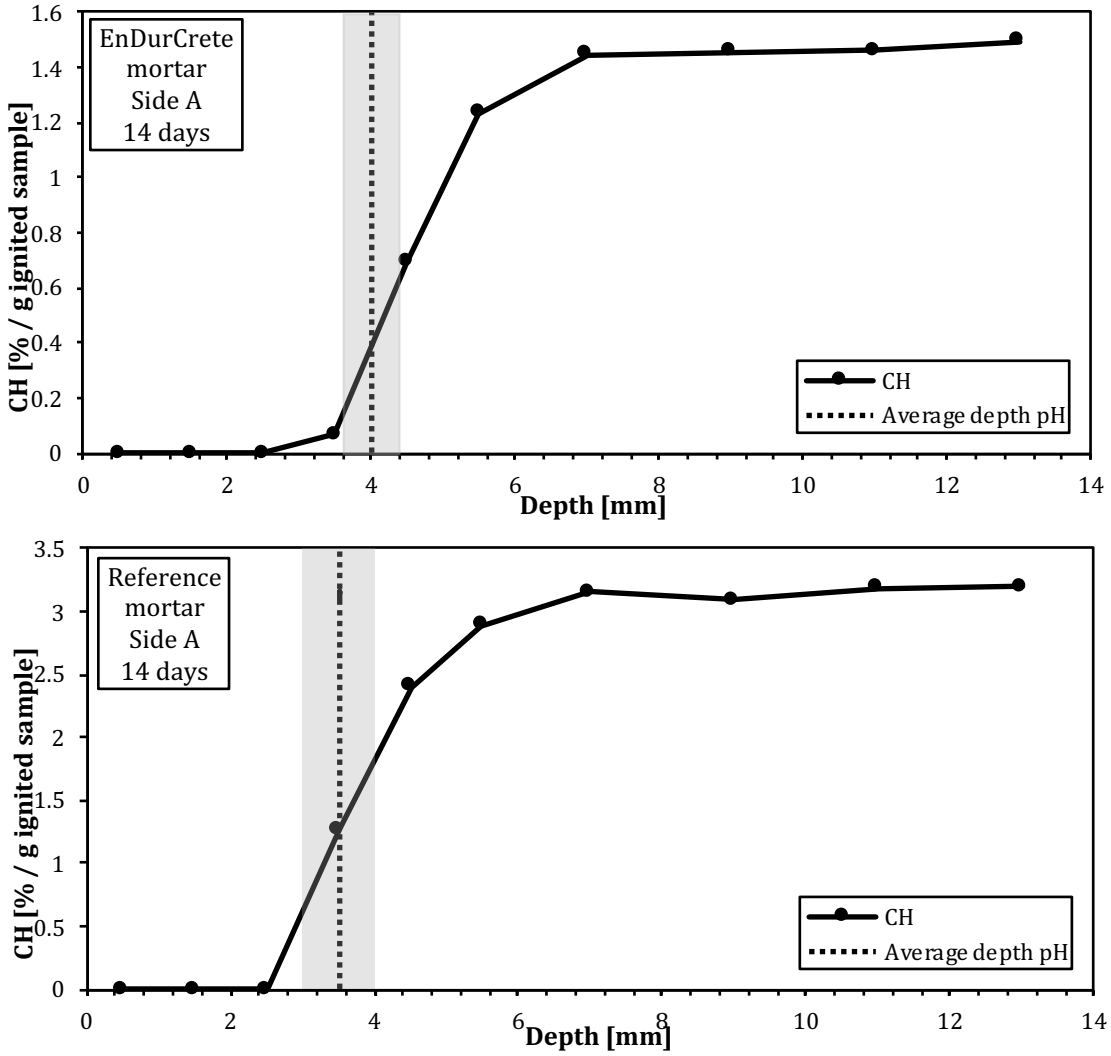

Figure 25 Comparison betweenthe average thymolphtalein carbonation depth and portlandite content from TGA. Top:EnDurCrete sample (E06M1-1 and E06M2-1). Bottom: Reference (R06M1-1 and R06M2-1) mortar after 14 days of exposure. The grey area represents the standard deviation for the thymolphtalein measurements.

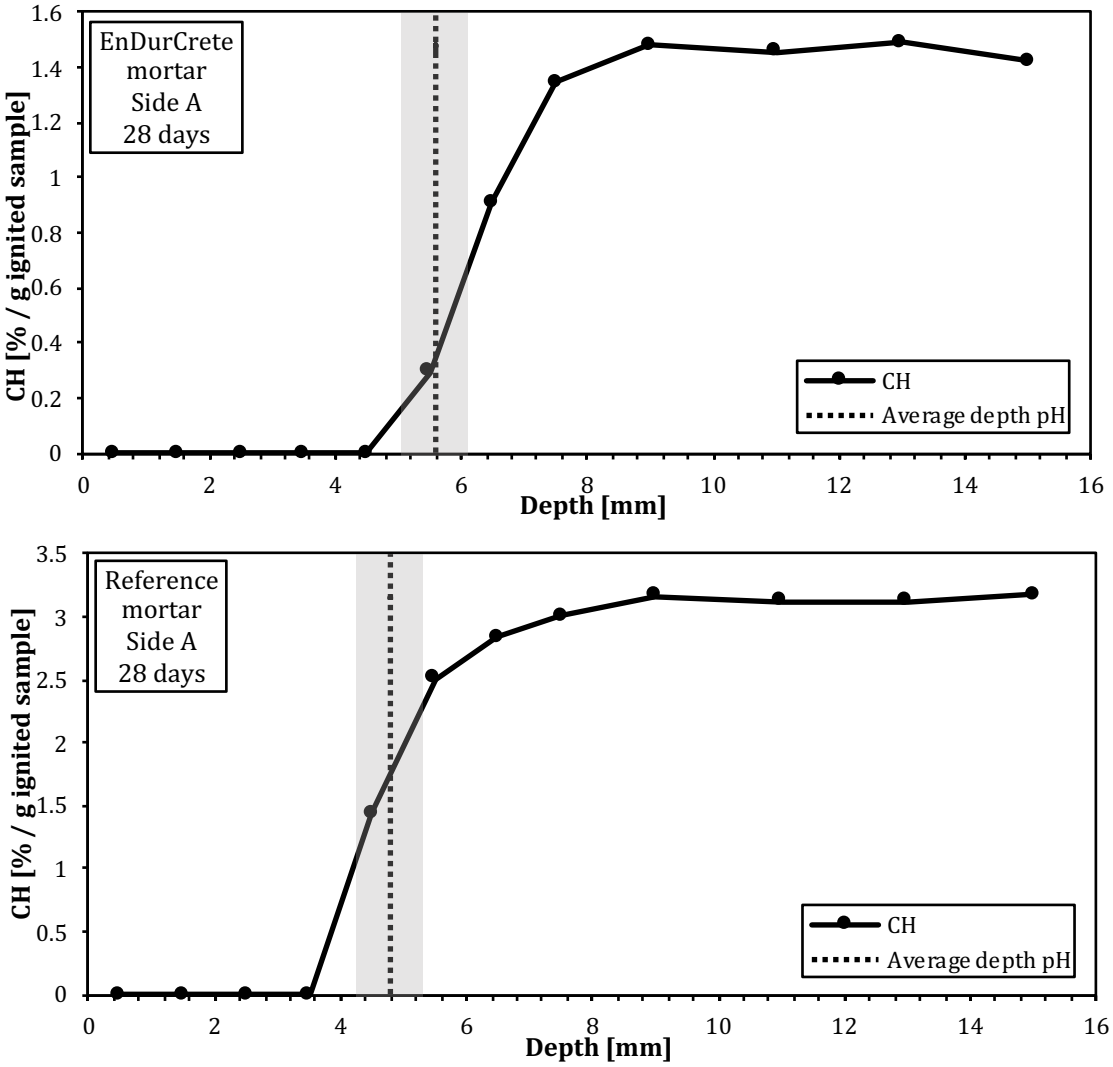

Figure 26 Comparison betweenthe average thymolphtalein carbonation depth and portlandite content from TGA. Top:EnDurCrete sample (E06M1-2 and E06M2-2). Bottom: Reference (R06M1-2 and R06M2-2) mortar after 28 days of exposure. The grey area represents the standard deviation for the thymolphtalein measurements.

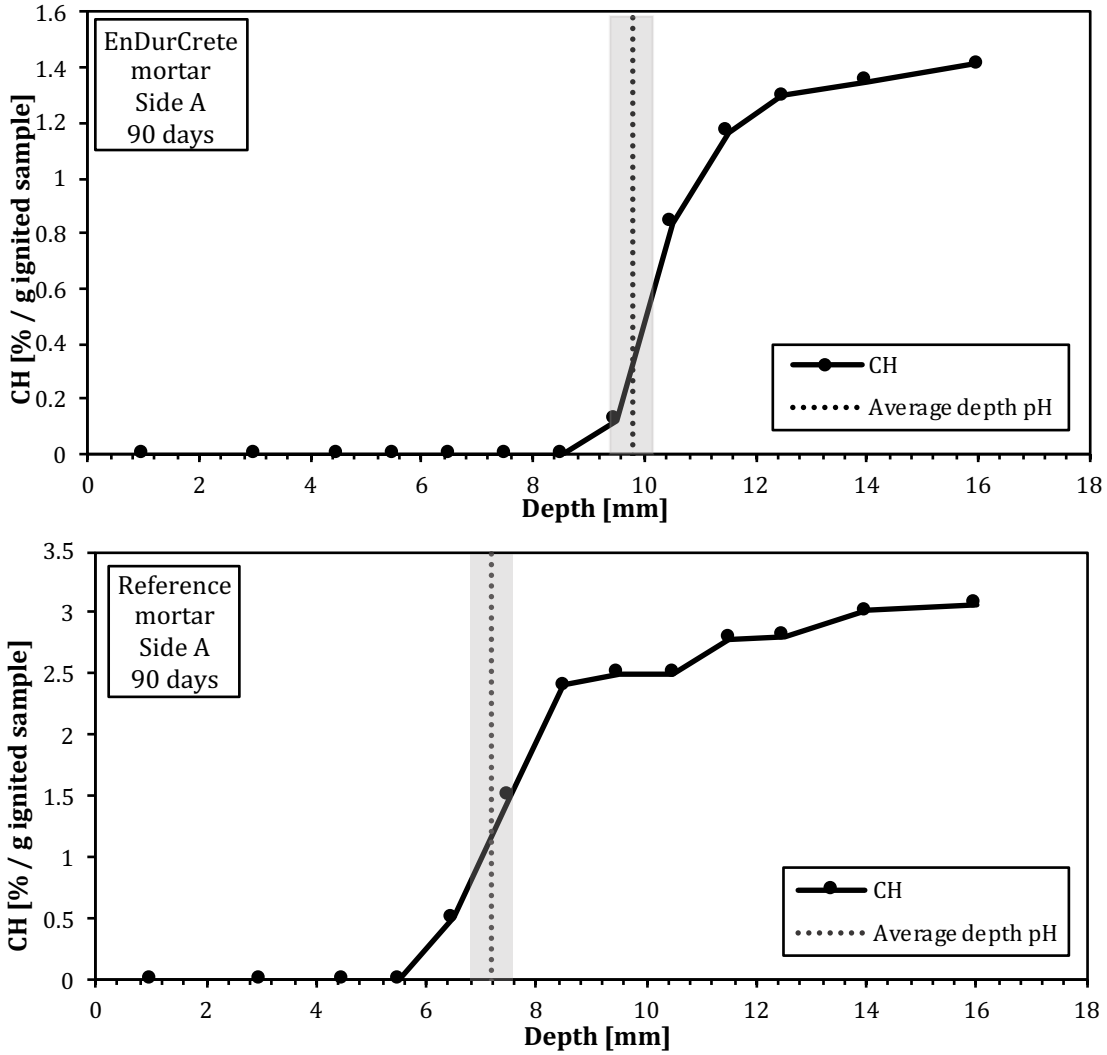

Figure 27 Comparison betweenthe average thymolphtalein carbonation depth and portlandite content from TGA. Top:EnDurCrete sample (E06M1-3 and E06M2-3). Bottom: Reference (R06M1-3 and R06M2-3) mortar after 90 days of exposure. The grey area represents the standard deviation for the thymolphtalein measurements.

When the sample is profile ground for TGA the spatial variations of the different phases are averaged because the sample is homogenized over the profile grinding step (1 or 2 mm). This effect of this is seen in the gradual change in portlandite content. Carbonation depht measurements with pH indicator show the spatial variations, but only for a limited part of the sample, i.e. the split surface (Figure 28). When the different methods of sampling are taken into consideration, the measurements are in good agreement with each other. The different sampling methods are illustrated in Figure 29.

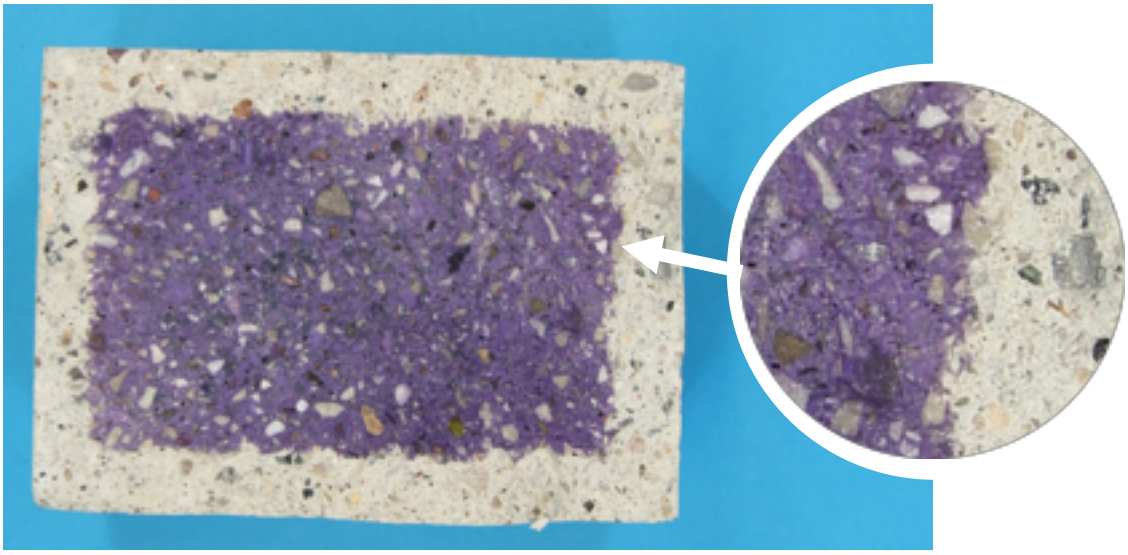

Figure 28 The spatial variation in the carbonation front in mortar sample E06M1-3 after 90 days.

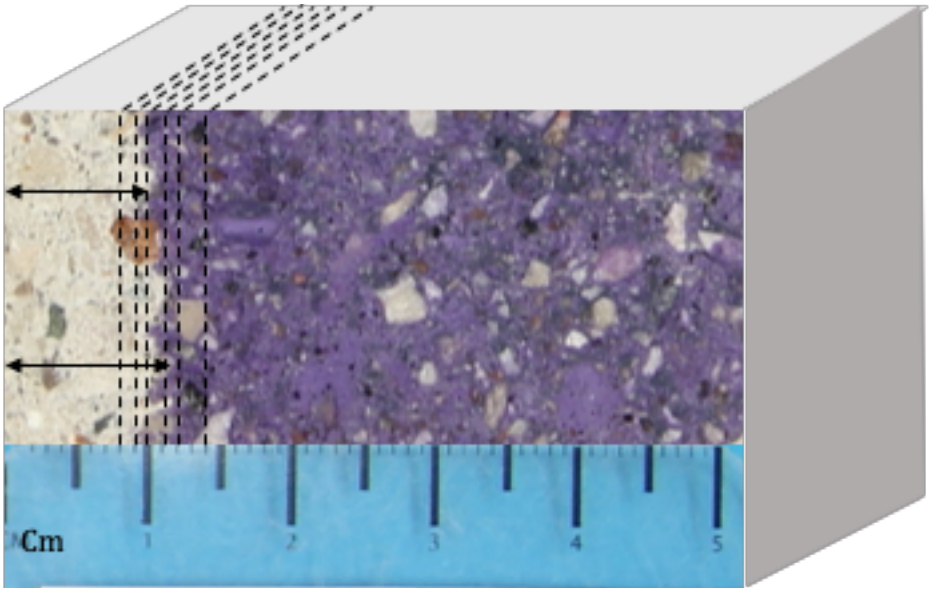

Figure 29 Illustration of the different sampling methods for measuring carboantion depth using thymolphtalein solution and profile grining for TGA. The black arrows indicate the carbonation depth measured perpendicular from the exposed surface to the colored carbonated area of the sample. The dashed lines show the volume of sample that is profileground in 1 mm steps and homogenized for TGA.

Figure 25, Figure 26 and Figure 27 show the location of the average depth using pH indicator relative to the transition from no CH to the CH plateau. The average depth using pH seems to be located closer to the depth where CH is zero for EnDurCrete samples, while for the reference samples it is closer to the middle of the transition between no CH and the first point of the plateau. This is explored further in Figure 30 and Figure 31.

Figure 30 visualizes where the average carbonation depth for the EnDurCrete mortar sample is located relative to CH content at the different exposure dates. The average depth from pH indicator is plotted together with the last point where the CH content is zero and the first point of the CH plateau. For the EnDurCrete sample the average

carbonation depth by pH indicator is closer to the depth where the CH content is zero, than the start of the plateau. The distance between them are similar over the entire exposure time. The standard deviations for the dotted lines in Figure 30 are half the size of the profile grinding step.

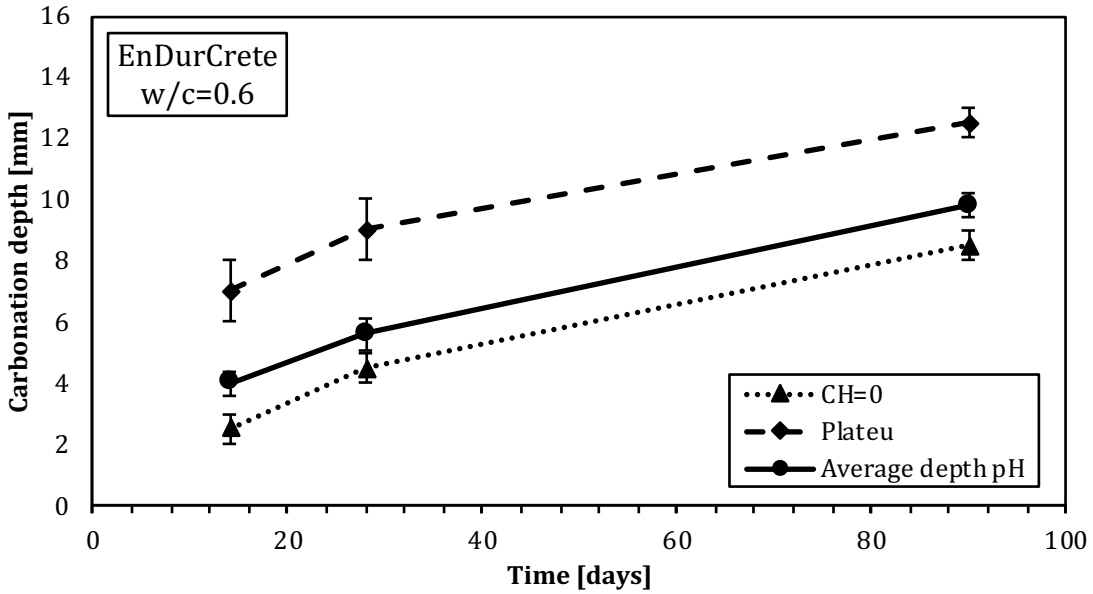

Figure 30 The average carbonation depth measured with pH indicator plotted against the last point where CH content is zero, and the first point in the CH plateau for EnDurCrete mortar samples (E06M1 and E06M2).

Figure 31 visualizes where the average carbonation depth for the reference mortar sample is located relative to CH content at the different exposure dates. The distance between the point where the CH content is zero and the average depth by pH remains even over the exposure time. The distance between the average depth by pH and the first point in the CH plateau however, decreases over the exposure time. Note that the 90 day plateau point for the reference is not from a clearly defined plateau, as seen in Figure 27. This made it difficult to define the first point of the plateau, possibly making the plateau point and the average pH depth appear closer to each other than they really are.

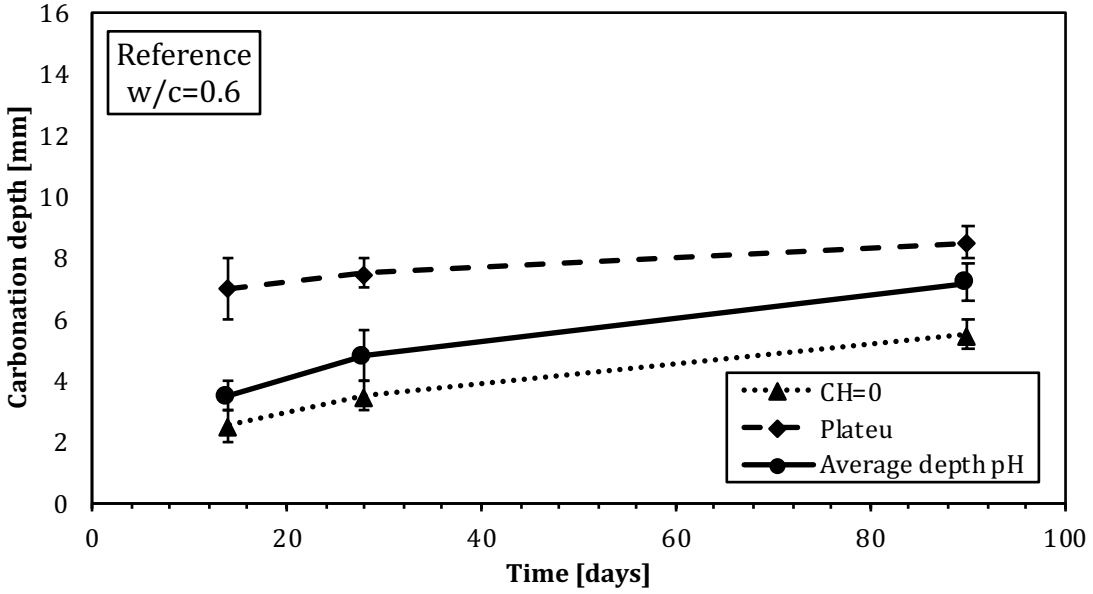

Figure 31 The average carbonation depth measured with pH indicator plotted against last point where CH content is zero, and the first point in the CH plateau for reference mortar samples (R06M1 and R06M2).

4.4. Relative humidity measurements

All the corrected values for the relative humidity are high. This indicates that the sample prisms were well sealed, so that the initial moisture state in the samples was preserved. Self dessication due to hydration causes the relative humidity to drop from 100 %, even though the samples were sealed. The self dessication is caused by the hydration reaction binding water in hydration products with smaller volume than the reactants. The relative humidity in the EnDurCrete samples and the reference samples are very similar, but the EnDurCrete concrete and mortar have a slightly lower value than the reference samples. The reason for this is most likely the higher content of SCMs in the EnDurCrete reacting further with the hydration products, as described in 1.3. The values for the relative humidity are in the same range as found by Lindgård et al. in [21] using a similar procedure for laboratory testing.

From the results for the corrected values the relative humidity of mortar and concrete samples agree well with each other. The difference is well within the accuracy of the humidity sensors (± 2% for up to 90% RH, ± 3% for 90-100 % RH). These results suggest that the relative humidity of mortar samples may be used to indicate the relative humidity in concrete samples. Performing the procedure for measuring relative humidity on mortar samples offers some advatntages compared to concrete. The mortar samples are easier to crush down, making gathering of sample material faster and limiting the time the sample material is exposed to drying. When crushing concrete samples, telling the difference between the mortar and aggregates may be difficult. In order to obtain reliable samples it is important to gather enough material, and therefore limit the amounts of aggregates in the sample.

5. Conclusions

The carbonation resistance of the low clinker cement developed by the EnDurCrete project (CEMII/C-M(S-LL)) was compared to a benchmark cement available in the European market (CEMII/A-S). In additon the relative humidity of the samples before exposure was determined. Tests were performed on both mortar and concrete samples.

- The portlandite content determined by TGA in mortar samples with the EnDurCrete cement that contains high levels of GGBFS, is significantly lower than for the reference cement containing smaller amounts of GGBFS. This is due to the lower clinker content and additional formation of C-S-H from the pozzolanic reaction of GGBFS.

- The carbonation ingress results on mortar and concrete agree well, except for the reference mortar samples which showed a lower carbonation ingress. The reason for this is unknown. Based on the carbonation ingress results obtained for concrete, the EnDurCrete concrete exhibits a similar carbonation resistance as the reference concrete with the commercially available reference cement.

- The carbonation depth determined by the pH indicator and the portlandite profiles agree well, taking into account the different ways of sampling for the two methods. The average carbonation depth using pH indicator is always in the transition between no CH and the CH plateau.

- The average RH for EnDurCrete mortar was 89.1 %, and for EnDurCrete concrete is was 88.4 %. The average RH for reference mortar was 91.8 %, and for reference concrete it was 91.3 %. This range of RH agrees with the level one would obtain by self-desiccation in sealed samples.

  The relative humidity is practically identical in concrete and mortar, making it possible to predict the moisture state in concrete by measuring the relative humidity in mortar samples.

6. Suggestions for further work

There are several interesting findings that were not discussed in this report that can be looked into in further studies.

Further research could be done into why some samples were carbonated more on the bottom and on the sides than at the top.

To improve the statistical quality of the measurements, the number of measuring points when measuring carbonation depth with pH indicator should be increased. After being sprayed with thymolphtalein the samples were photographed with a scale, allowing for the carbonation depth to be studied in more detail at a later time using image analysis.

The reason for why the TGA results showed a lower bound water content for the 90 days exposure than for the other two measurement dates should aslo be looked in to.

A study of porosity and its effect on carbonation should be performed to obtain more information on the carbonation resistance of the EnDurCrete and reference cement, and possibly explain why the reference mortar is less carbonated than the rest of the samples.

In addition to accelerated tests in laboratory, field testing of the concrete should be performed. This will be done in the EnDurCrete project.

7. References

1. Andrew, R.M., *Global CO 2 emissions from cement production.* Earth System Science Data, 2018. **10**(1): p. 195-217.
2. Norcem. *Cement production and CO2*. [cited 2019 09.25].
3. Kjellsen, K.O., *Chapter 5 - Cement*, in *TKT 4215 : Concrete technology 1*, S. Jacobsen, Editor. 2011, Norwegian University of Science and Technology, Faculty of Engineering Science and Technology, Department of Structural Engineering: Trondheim.
4. Scrivener, K.L., V.M. John, and E.M. Gartner, *Eco-efficient cements: Potential economically viable solutions for a low-CO2 cement-based materials industry.* Cement and Concrete Research, 2018. **114**: p. 2-26.
5. Sellevold, E.J., *Chapter 6 - Hydration*, in *TKT 4215 : Concrete technology 1*, S. Jacobsen, Editor. 2011, Norwegian University of Science and Technology, Faculty of Engineering Science and Technology, Department of Structural Engineering: Trondheim.
6. Taylor, H.F.W., *Cement chemistry*. 1990, London: Academic Press.
7. Bertolini, L., et al., *Chapter 5: Carbonation-induced corrosion*, in *Corrosion of steel in concrete: prevention, diagnosis, repair*. 2013, Wiley-VCH: Weinheim.
8. Tuutti, K., *Corrosion of steel in concrete*. 1982.
9. Sellevold, E.J., *Chapter 14 - Permeability, moisture condition*, in *TKT 4215 : Concrete technology 1*, S. Jacobsen, Editor. 2011, Norwegian University of Science and Technology, Faculty of Engineering Science and Technology, Department of Structural Engineering: Trondheim.
10. Lothenbach, B., K. Scrivener, and R.D. Hooton, *Supplementary cementitious materials.* Cement and Concrete Research, 2011. **41**(3): p. 217-229.
11. *NS-EN 12390-2:2009 Testing hardened concrete*, in *Part 2: Making and curing specimens for strength tests*. 2009, Standard Norge.
12. De Weerdt, K., et al., *Effect of carbonation on the pore solution of mortar.(Report).* Cement and Concrete Research, 2019. **118**: p. 38.
13. *NS-EN 13295 Products and systems for the protection and repair of concrete structures, Test methods, Determination of restistance to carbonation*. 2004, Standard Norge.
14. Revert, A.B., et al., *Carbonation Characterization of Mortar with Portland Cement and Fly Ash, Comparison of Techniques* 2018, NTNU.
15. Lothenbach, B., P. Durdziński, and K. De Weerdt, *Thermogravimetric Analysis*, in *A Practical Guide to Microstructural Analysis of Cementitious Materials*, K. Scrivener, R. Snellings, and B. Lothenbach, Editors. 2016. p. 177-211.
16. Leemann, A., et al., *Relation between carbonation resistance, mix design and exposure of mortar and concrete.* Cement and Concrete Composites, 2015. **62**: p. 33-43.
17. Scrivener, K., A. Crumbie, and P. Laugesen, *The Interfacial Transition Zone (ITZ) Between Cement Paste and Aggregate in Concrete.* Interface Science, 2004. **12**(4): p. 411-421.
18. Han, J., et al., *Effects of crack and ITZ and aggregate on carbonation penetration based on 3D micro X-ray CT microstructure evolution.* Construction and Building Materials, 2016. **128**: p. 256-271.

19. Elsharief, A., M.D. Cohen, and J. Olek, *Influence of aggregate size, water cement ratio and age on the microstructure of the interfacial transition zone.* Cement and Concrete Research, 2003. **33**(11): p. 1837-1849.
20. *Official Journal of the European Union L 353, 31.12.2008 : Regulation (EC) No 1272/2008 of the European Parliament and of the Council of 16 December 2008 on classification, labelling and packaging of substances and mixtures, amending and repealing Directives 67/548/EEC and 1999/45/EC, and amending Regulation (EC) No 1907/2006.* Official Journal of the European Union L 353, 31.12.2008 : Regulation (EC) No 1272/2008 of the European Parliament and of the Council of 16 December 2008 on classification, labelling and packaging of substances and mixtures, amending and repealing Directives 67/548/EEC and 1999/45/EC, and amending Regulation (EC) No 1907/2006., 2008.
21. Lindgård, J., et al., *Alkali–silica reaction (ASR)—performance testing: Influence of specimen pre-treatment, exposure conditions and prism size on concrete porosity, moisture state and transport properties.* 2013.

8. Appendices

8.1. Appendix A: Carbonation depth measurements with pH indicator

All measurements of carbonation depth with pH indicator taken for all samples are presented in the Table A.1, Table A.2, Table A.3 and Table A.4 below.

Table A.1: Measurements for EnDurCrete mortar sample with w/c 0.6, for 14, 28 and 90 days of exposure.

Date of casting	Exposure start	Sample name	Exposure time	Date of measurement	Side	Carbonation depth at measurement point [mm]					Average [mm]	Standard deviation [mm]
						1	2	3	4	5		
12.-15.02.19	30.04.19	E06M1-1	14 d	14.05.19	Side A	4	3.5	4	4	4.5	4.0	0.4
					Top	4.5	4	5	5	4	4.5	0.5
					Side C	3.5	3.5	4.5	4	5	4.1	0.7
					Bottom	4	4	3.5	3	3	3.5	0.5
		E06M1-2	28 d	28.05.19	Side A	6	6	5	6	5	5.6	0.5
					Top	5.5	5.5	6.5	6	6	5.9	0.4
					Side C	6	6	6	5	5.5	5.7	0.4
					Bottom	5	6	5.5	5	5	5.3	0.4
		E06M1-3	90 d	29.07.19	Side A	10	10	9	10	10	9.8	0.4
					Top	10	10	11	12	10	10.6	0.9
					Side C	10	9.5	9.5	10	10	9.8	0.3
					Bottom	9	8	8.5	8.5	9	8.6	0.4

Table A.2: Measurements of carbonation depth with pH indicator for EnDurCrete concrete sample with w/c 0.6, for 14, 28 and 90 days of exposure.

Date of casting	Exposure start	Sample name	Exposure time	Date of measurement	Side	Carbonation depth at measurement point [mm]					Average [mm]	Standard deviation [mm]
						1	2	3	4	5		
12.-15.02.19	30.04.19	E06C-1	14 d	14.05.19	Side A	4	5	4	3.5	4	4.1	0.5
					Top	3.5	4.5	x	4	x	4.0	0.5
					Side C	x	4	3	3.5	4	3.6	0.5
					Bottom	3.5	3.5	3.5	3	x	3.4	0.3
		E06C-2	28 d	28.05.19	Side A	6	4	x	5	5	5.0	0.8
					Top	x	x	x	6	6	6.0	0.0
					Side C	6	5	3	4	5	4.6	1.1
					Bottom	5	5.5	4.5	5	4	4.8	0.6
		E06C-3	90 d	29.07.19	Side A	9	9	8.5	10	x	9.1	0.6
					Top	x	x	9	9	x	9.0	0.0
					Side C	8	8.5	9	9	9	8.7	0.4
					Bottom	x	7.5	8	x	x	7.8	0.4

Table A.3: Measurements of carbonation depth with pH indicator for reference mortar sample with w/c 0.6, for 14, 28 and 90 days of exposure.

Date of casting	Exposure start	Sample name	Exposure time	Date of measurement	Side	Carbonation depth at measurement point [mm]					Average [mm]	Standard deviation [mm]
						1	2	3	4	5		
12.-15.02.19	30.04.19	R06M1-1	14 d	14.05.19	Side A	1	2	3	4	5	3.5	0.5
					Top	4	3	4	3	3.5	3.2	0.3
					Side C	3	3	3	3.5	3.5	3.3	0.3
					Bottom	3.5	3.5	3.5	3	3	2.5	0.7
		R06M1-2	28 d	28.05.19	Side A	2	2	3.5	3	2	4.8	0.6
					Top	4.5	5	5	5.5	4	4.3	0.3
					Side C	4.5	4.5	4.5	4	4	5.1	0.7
					Bottom	4.5	5.5	4.5	5	6	3.3	0.3
		R06M1-3	90 d	29.07.19	Side A	3.5	x	3.5	3	3	7.2	0.4
					Top	7	7	7	7	8	7.2	0.9
					Side C	7.5	8	8	6.5	6	7.5	0.5
					Bottom	8	8	7.5	7	7	4.2	0.9

Table A.4: Measurements of carbonation depth with pH indicator for reference concrete sample with w/c 0.6, for 14, 28 and 90 days of exposure.

Date of casting	Exposure start	Sample name	Exposure time	Date of measurement	Side	Carbonation depth at measurement point [mm]					Average [mm]	Standard deviation [mm]
						1	2	3	4	5		
12.-15.02.19	30.04.19	R06C-1	14 d	14.05.19	Side A	x	5	4	5	x	4.7	0.6
					Top	4	5	4	3.5	3.5	4	0.6
					Side C	x	5	5	3.5	4	4.4	0.8
					Bottom	3.5	3.5	x	3.5	3	3.4	0.3
		R06C-2	28 d	28.05.19	Side A	5	5	5	5	4.5	4.9	0.2
					Top	3.5	4	5	5	x	4.4	0.8
					Side C	x	5	4	5	x	4.8	0.4
					Bottom	4	5	4	3.5	3.5	5.0	0.0
		R06C-3	90 d	29.07.19	Side A	x	5	5	3.5	4	8.6	0.3
					Top	3.5	3.5	x	3.5	3	7.1	1.1
					Side C	5	5	5	5	4.5	8.1	0.9
					Bottom	3.5	4	5	5	x	9.3	1.2

8.2. Appendix B: Calibration results, calibration curves, measured values and corrected values for relative humidity

8.2.1. Appendix B.1: Calibration results

Table B.1: Results from calibration performed in March 2019, before measurement period.

	Reference RH					
Sensor ID	**75.4 %**	**80.0 %**	**85.1 %**	**90.0 %**	**95.1 %**	**20.0°C**
C4050001	72.0	76.7	82.0	87.4	92.5	19.8
C3950019	71.9	76.5	81.7	87.0	92.3	19.9
C4050004	76.2	77.3	82.6	88.0	93.4	19.9
C3950018	72.1	76.9	82.2	87.6	93.2	19.8
E4330005	72.8	77.6	83.1	88.7	94.5	19.8
E150002	71.9	76.6	81.9	87.2	92.6	20.0
F3340019	75.0	80.1	85.5	91.5	97.5	19.9
C4050002	72.0	76.5	81.7	87.1	92.6	19.7
C4050007	69.1	73.7	78.6	84.0	89.2	19.8
C3950015	72.0	76.8	82.1	87.0	92.8	19.7
G2620002	79.7	84.9	90.4	96.3	101.8	19.6

Table B.2: Results from calibration performed in May 2019, after measurement period.

	Reference RH					
Sensor ID	**75.4 %**	**80.0 %**	**85.1 %**	**90.0 %**	**95.1 %**	**20.0°C**
C3950015	72.1	76.8	82.2	87.5	92.5	19.7
C3950019	72.3	77.0	82.1	87.1	92.3	19.9
C4050001	72.4	77.1	82.2	87.3	92.4	19.8
E4330005	73.0	77.7	83.1	88.5	94.2	19.8
E150002	72.1	76.7	81.8	86.8	92.1	20.0
C4050007	73.4	78.1	83.3	84.5	89.6	19.7
C4050004	73.4	78.1	83.3	88.4	93.7	19.8
C3950018	72.4	77.2	82.4	87.6	93.1	19.8
C4050002	72.7	77.2	82.5	86.2	92.8	19.7
F3340019	75.6	80.7	86.2	91.8	97.8	19.8
G2620002	80.8	85.9	91.4	96.7	101.7	19.6

8.2.2. Appendix B.2: Calibration curves

Plots of the calibration results for all sensors fitted with linear trendline and the equation for the trend lines is presented in Figure B.1 – Figure B.11.

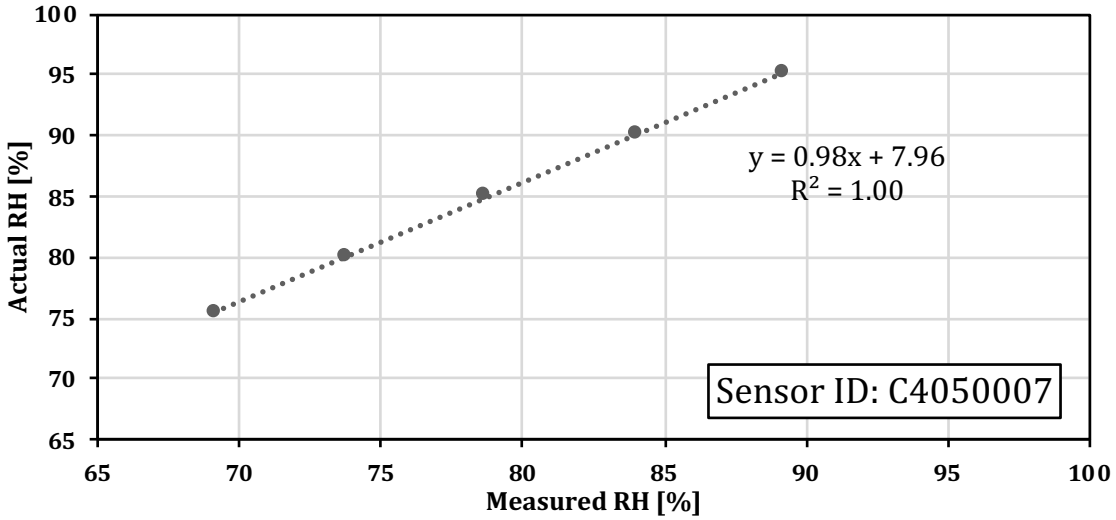

Figure B.1: Calibration curve for sensor C4050007.

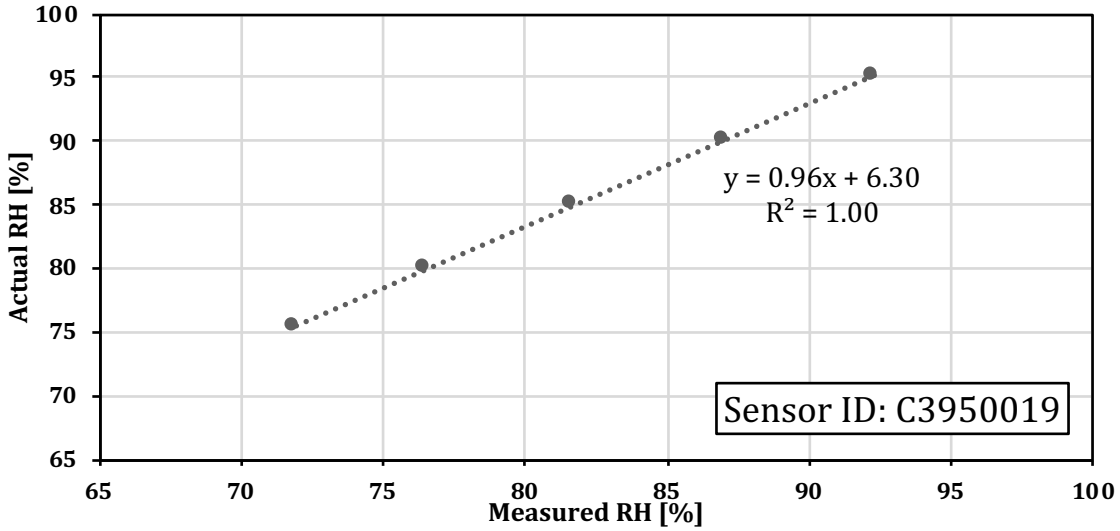

Figure B.2: Calibration curve for sensor C3950019.

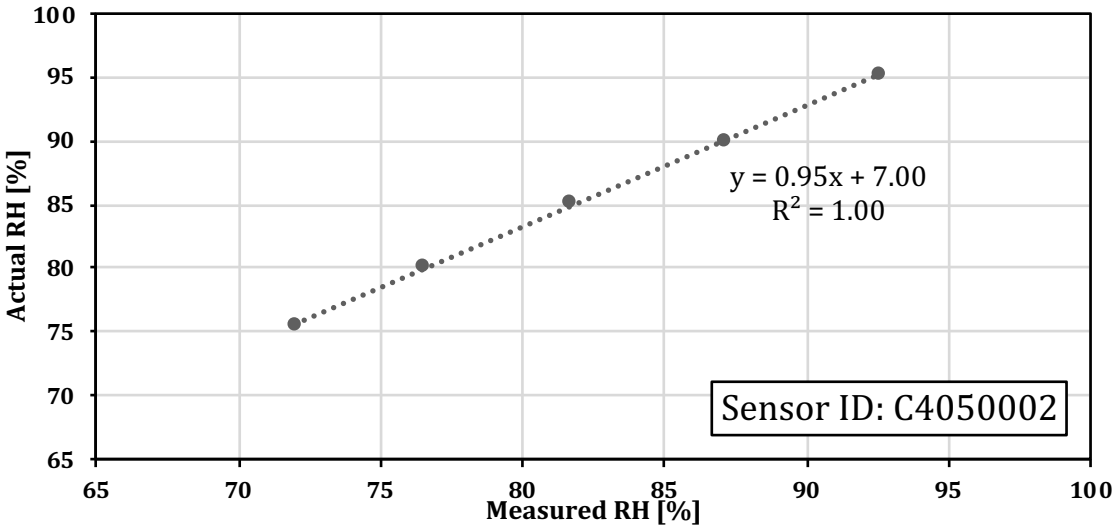

Figure B.3: Calibration curve for sensor C4050002.

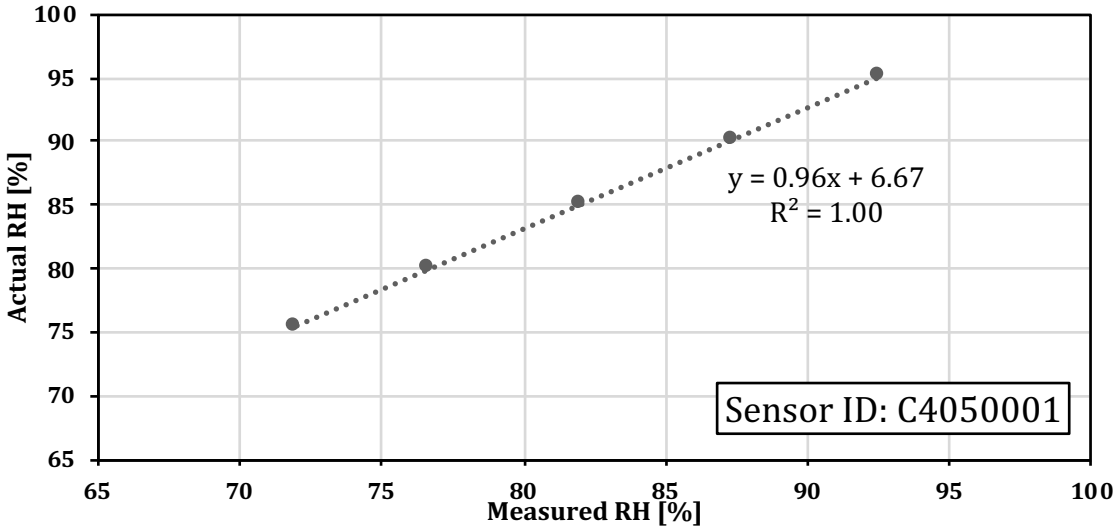

Figure B.4: Calibration curve for sensor C4050001.

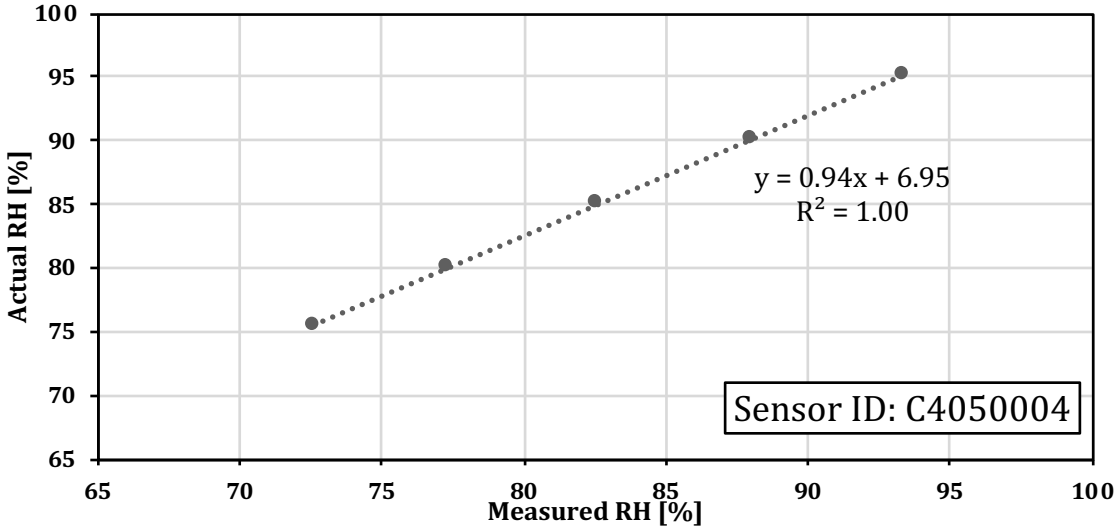

Figure B.5: Calibration curve for sensor C4050004.

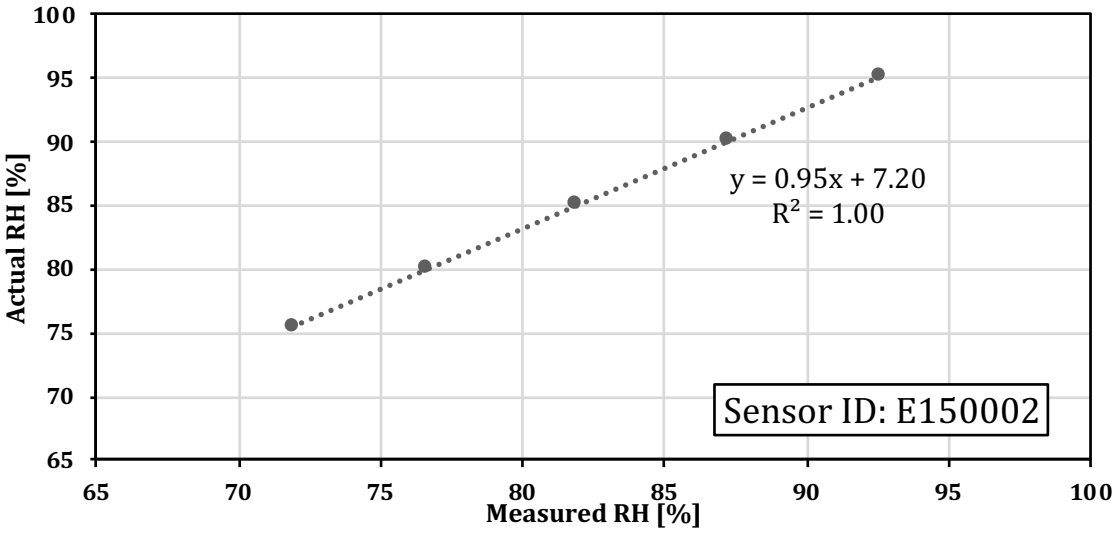

Figure B.6: Calibration curve for sensor E150002.

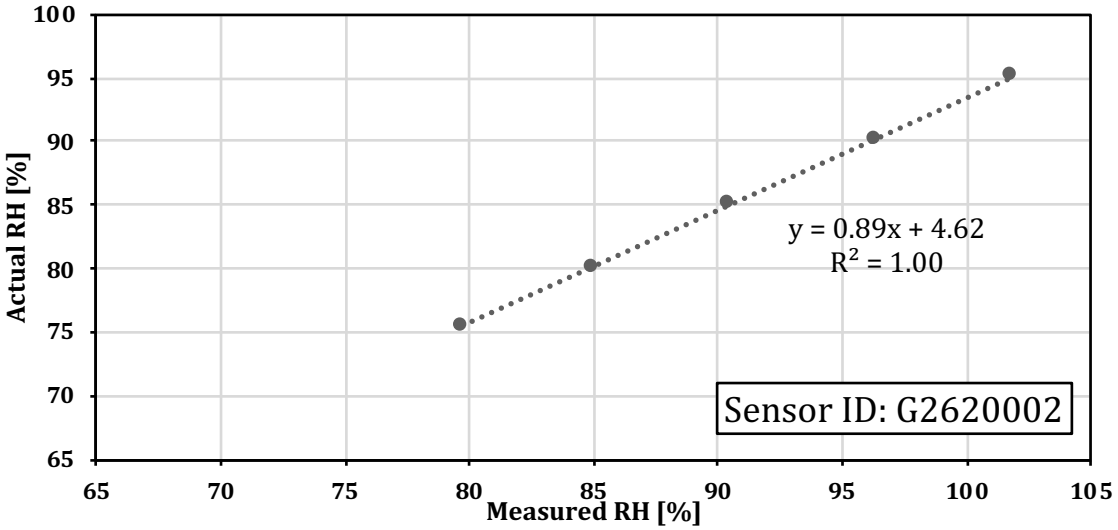

Figure B.7: Calibration curve for sensor G2620002.

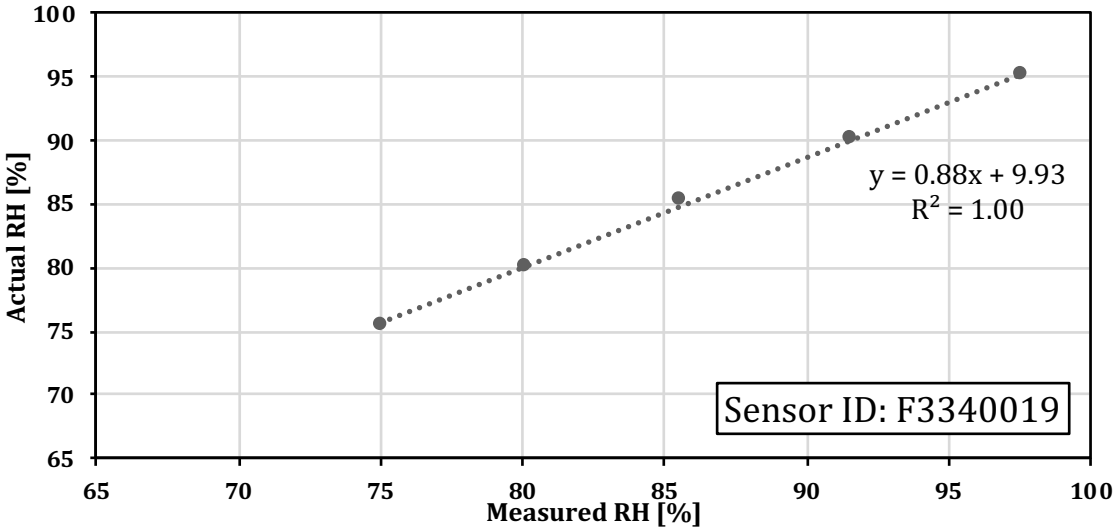

Figure B.8: Calibration curve for sensor F3340019.

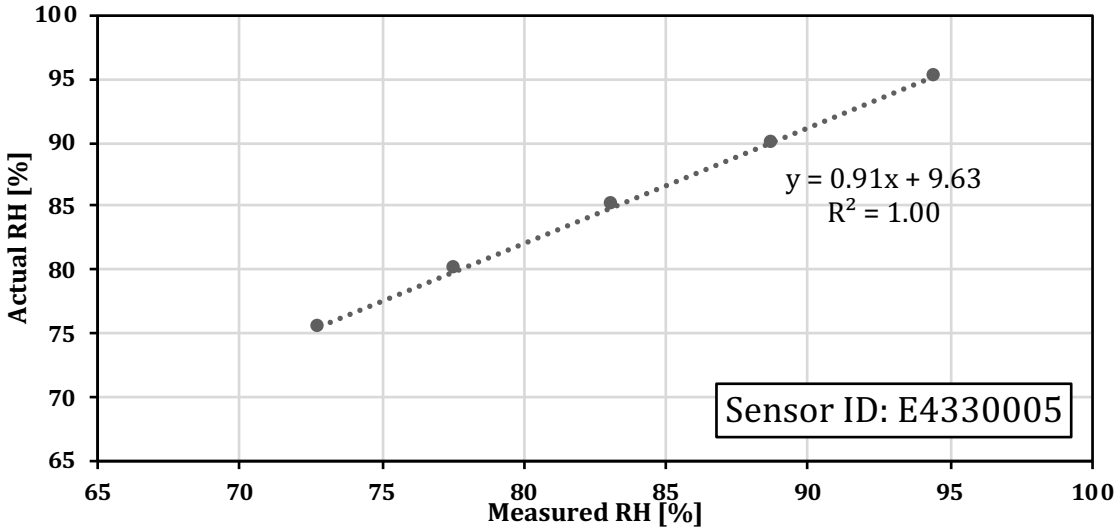

Figure B.9: Calibration curve for sensor E4330005.

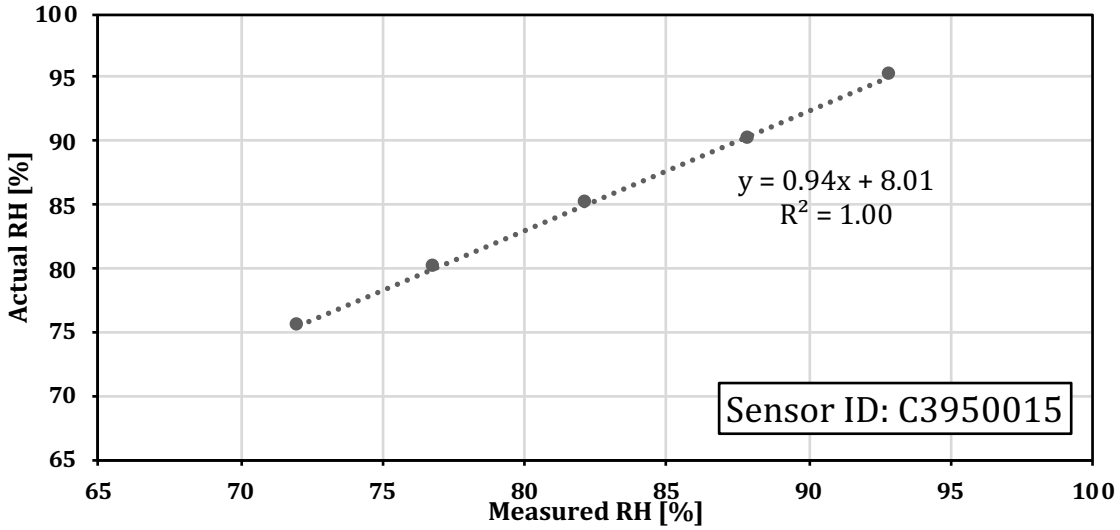

Figure B.10: Calibration curve for sensor C3950015.

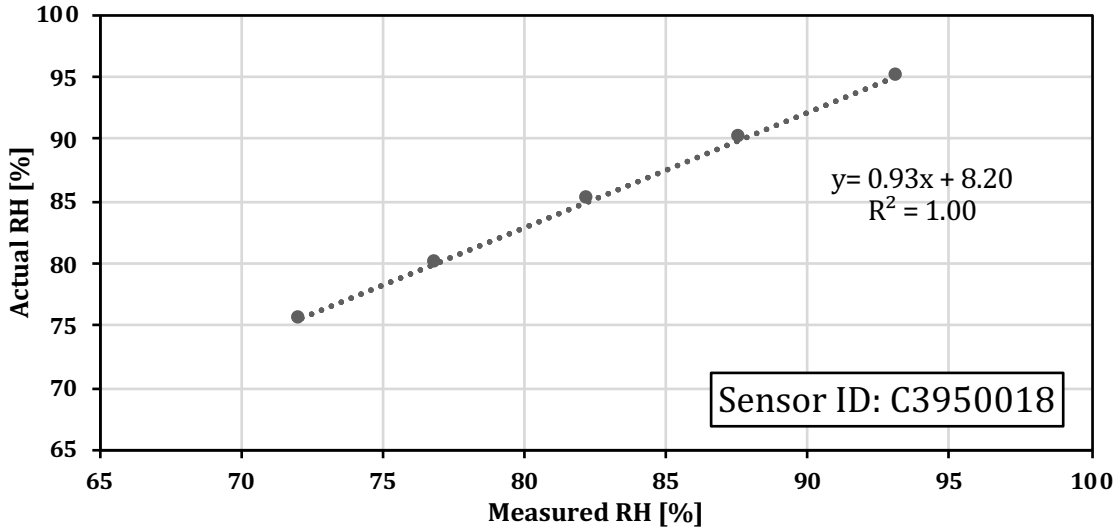

Figure B.11: Calibration curve for sensor C3950018.

8.2.3. Appendix B.3: Measurements and corrected values

All measurements performed on the concrete and mortar samples with EnDurCrete and reference cement are given in Table B.3 – Table B.12. The corrected values calculated using the equation of the linear trendline for the corresponding sensor are aslo given in the tables. Operators: Alisa Machner (AM), Marie H. Bjørndal (MB).

Table B.3: RH measurements and corrected values for EnDurCrete mortar sample no. 1, with w/c 0.6.

Sample name	RH_E0.6M#1	EnDurCrete w/c 0.6, mortar sample no.1.			
Sensor ID	C4050007				
	Date	**Operator**	**RH-meas. [%]**	**T-meas. [ºC]**	**RH-corr. [%]**
Sample prep.	06.05.2019				
1days	07.05.2019	AM+MB	81.4	21.1	87.5
2 days	08.05.2019	AM	81.7	21.1	87.8
3 days	09.05.2019	AM	81.7	21.4	87.8
4 days	10.05.2019	MB	81.7	21.3	87.8
				Average (2-4 days)	**87.84**
				stdev	0.0

Table B.4: RH measurements and corrected values for EnDurCrete mortar sample no. 2, with w/c 0.6.

Sample name	RH_E0.6M#2	EnDurCrete w/c 0.6, mortar sample no.2.			
Sensor ID	C3950019				
	Date	**Operator**	**RH-meas. [%]**	**T-meas. [ºC]**	**RH-corr. [%]**
Sample prep.	06.05.2019				
1days	07.05.2019	AM+MB	86.4	21.1	89.5
2 days	08.05.2019	AM	86.7	21.1	89.8
3 days	09.05.2019	AM	86.7	21.4	89.8
4 days	10.05.2019	MB	86.7	21.3	89.8
				Average (2-4 days)	**89.76**
				stdev	0.0

Table B.5: RH measurements and corrected values for EnDurCrete mortar sample no. 3, with w/c 0.6.

Sample name	RH_E0.6M#3	EnDurCrete w/c 0.6, mortar sample no.3.			
Sensor ID	C4050002				
	Date	**Operator**	**RH-meas. [%]**	**T-meas. [ºC]**	**RH-corr. [%]**
Sample prep 0 days	06.05.2019				
1days	07.05.2019	AM+MB	86.9	21.1	89.8
2 days	08.05.2019	AM	87	21	89.9
3 days	09.05.2019	AM	86.9	21.3	89.8
4 days	10.05.2019	MB	86.9	21.2	89.8
				Average (2-4 days)	**89.84**
				stdev	0.1

Table B.6: RH measurements and corrected values for EnDurCrete concrete sample no. 1, with w/c 0.6.

Sample name	RH_E0.6C#1	EnDurCrete w/c 0.6, concrete sample no.1.			
Sensor ID	C4050001				
	Date	**Operator**	**RH-meas. [%]**	**T-meas. [ºC]**	**RH-corr. [%]**
Sample prep 0 days	06.05.2019				
1days	07.05.2019	AM+MB	83.9	21.1	86.8
2 days	08.05.2019	AM	84.3	20.9	87.2
3 days	09.05.2019	AM	84.2	21.2	87.1
4 days	10.05.2019	MB	84.1	21.2	87.0
				Average (2-4 days)	**87.11**
				stdev	0.1

Table B.7: RH measurements and corrected values for EnDurCrete concrete sample no. 2, with w/c 0.6.

Sample name	RH_E0.6C#2	EnDurCrete w/c 0.6, concrete sample no.2.			
Sensor ID	C4050004				
	Date	**Operator**	**RH-meas. [%]**	**T-meas. [ºC]**	**RH-corr. [%]**
Sample prep 0 days	06.05.2019				
1days	07.05.2019	AM+MB	87.4	21.2	89.5
2 days	08.05.2019	AM	87.6	21	89.7
3 days	09.05.2019	AM	87.5	21.3	89.6
4 days	10.05.2019	MB	87.5	21.2	89.6
				Average (2-4 days)	**89.61**
				stdev	0.1

Table B.8: RH measurements and corrected values for reference mortar sample no. 1, with w/c 0.6.

Sample name	RH_R0.6M#1	Reference w/c 0.6, mortar sample no. 1.			
Sensor ID	E150002				
	Date	**Operator**	**RH-meas. [%]**	**T-meas. [ºC]**	**RH-corr. [%]**
Sample prep 0 days	08.04.2019				
1days	09.04.2019	AM+MB	87.8	21.3	90.6
2 days	10.04.2019	AM	88.1	21.3	90.9
3 days	11.04.2019	AM	88.8	21.6	91.5
4 days	12.04.2019	MB	87.9	21.5	90.7
				Average (2-4 days)	**91.04**
				stdev	0.4

Table B.9: RH measurements and corrected values for reference mortar sample no. 2, with w/c 0.6.

Sample name	RH_R0.6M#2	Reference w/c 0.6, concrete sample no.2.			
Sensor ID	G2620002				
	Date	**Operator**	**RH-meas. [%]**	**T-meas. [ºC]**	**RH-corr. [%]**
Sample prep 0 days	08.04.2019				
1days	09.04.2019	AM+MB	97.8	21.1	91.5
2 days	10.04.2019	AM	98.5	21	92.1
3 days	11.04.2019	AM	98.6	21.4	92.2
4 days	12.04.2019	MB	98.8	21.3	92.4
				Average (2-4 days)	**92.24**
				stdev	0.1

Table B.10: RH measurements and corrected values for reference mortar sample no. 3, with w/c 0.6.

Sample name	RH_R0.6M#3	Reference w/c 0.6, mortar sample no.3.			
Sensor ID	F3340019				
	Date	**Operator**	**RH-meas. [%]**	**T-meas. [ºC]**	**RH-corr. [%]**
Sample prep:	08.04.2019				
1days	09.04.2019	AM+MB	93.6	21.4	91.8
2 days	10.04.2019	AM	93.9	21.3	92.1
3 days	11.04.2019	AM	93.7	21.6	91.9
4 days	12.04.2019	MB	93.8	21.5	92.0
				Average (2-4 days)	**92.01**
				stdev	0.1

Table B.11: RH measurements and corrected values for reference concrete sample no.1, with w/c 0.6.

Sample name	RH_R0.6C#1	Reference w/c 0.6, concrete sample no.1.			
Sensor ID	E4330005				
	Date	**Operator**	**RH-meas. [%]**	**T-meas. [ºC]**	**RH-corr. [%]**
Sample prep:	08.04.2019				
1days	09.04.2019	AM+MB	90.1	21.2	91.2
2 days	10.04.2019	AM	90.3	21.1	91.4
3 days	11.04.2019	AM	90.3	21.4	91.4
4 days	12.04.2019	MB	90.2	21.3	91.3
				Average (2-4 days)	**91.40**
				stdev	0.1

Table B.12: RH measurements and corrected values for reference concrete sample no. 2, with w/c 0.6.

Sample name	RH_R0.6C#1	Reference w/c 0.6, concrete sample no.2.			
Sensor ID	E4330005				
	Date	**Operator**	**RH-meas. [%]**	**T-meas. [ºC]**	**RH-corr. [%]**
Sample prep:	08.04.2019				
1days	09.04.2019	AM+MB	90.1	21.2	91.2
2 days	10.04.2019	AM	90.3	21.1	91.4
3 days	11.04.2019	AM	90.3	21.4	91.4
4 days	12.04.2019	MB	90.2	21.3	91.3
				Average (2-4 days)	**91.40**
				stdev	0.1